RADC-TR-90-17
Final Technical Report
April 1990

OPTIMAL PHASE-ONLY FILTERS

Carnegie Mellon University

B.V.K.Vijaya Kumar and Z. Bahri

APPROVED FOR PUBLIC RELEASE; DISTRIBUTION UNLIMITED.

Rome Air Development Center
Air Force Systems Command
Griffiss Air Force Base, NY 13441-5700

This report has been reviewed by the RADC Public Affairs Division (PA) and is releasable to the National Technical Information Services (NTIS) At NTIS it will be releasable to the general public, including foreign nations.

RADC-TR-90-17 has been reviewed and is approved for publication.

APPROVED: Joseph J Horner

JOSEPH HORNER
Project Engineer

APPROVED: Harold Roth

HAROLD ROTH
Director of Solid State Sciences

FOR THE COMMANDER: James W. Hyde III

JAMES W. HYDE III
Directorate of Plans & Programs

If your address has changed or if you wish to be removed from the RADC mailing list, or if the addressee is no longer employed by your organization, please notify RADC (ESO) Hanscom AFB MA 01731-5000 This will assist us in maintaining a current mailing list.

Do not return copies of this report unless contractual obligations or notices on a specific document require that it be returned.

UNCLASSIFIED
SECURITY CLASSIFICATION OF THIS PAGE

REPORT DOCUMENTATION PAGE

Form Approved OMB No. 0704-0188

1a REPORT SECURITY CLASSIFICATION UNCLASSIFIED	1b RESTRICTIVE MARKINGS N/A
2a SECURITY CLASSIFICATION AUTHORITY N/A	3 DISTRIBUTION/AVAILABILITY OF REPORT Approved for public release; distribution unlimited.
2b DECLASSIFICATION/DOWNGRADING SCHEDULE N/A	
4 PERFORMING ORGANIZATION REPORT NUMBER(S) N/A	5 MONITORING ORGANIZATION REPORT NUMBER(S) RADC-TR-90-17
6a NAME OF PERFORMING ORGANIZATION Carnegie Mellon University 6b OFFICE SYMBOL (If applicable)	7a NAME OF MONITORING ORGANIZATION Rome Air Development Center (ESO)
6c ADDRESS (City, State, and ZIP Code) Department of Electrical and Computer Engineering Pittsburgh PA 15213-2454	7b ADDRESS (City, State, and ZIP Code) Hanscom AFB MA 01731-5000
8a NAME OF FUNDING/SPONSORING ORGANIZATION Rome Air Development Center 8b OFFICE SYMBOL (If applicable) ESO	9 PROCUREMENT INSTRUMENT IDENTIFICATION NUMBER F19628-88-K-0018
8c ADDRESS (City, State, and ZIP Code) Hanscom AFB MA 01731-5000	10 SOURCE OF FUNDING NUMBERS PROGRAM ELEMENT NO: 61102F; PROJECT NO: 2305; TASK NO: J7; WORK UNIT ACCESSION NO: J5

11 TITLE (Include Security Classification)
OPTIMAL PHASE-ONLY FILTERS

12 PERSONAL AUTHOR(S)
B. V. K. Vijaya Kumar, Z. Bahri

13a TYPE OF REPORT	13b TIME COVERED	14 DATE OF REPORT (Year, Month, Day)	15 PAGE COUNT
Final	FROM Apr 88 TO Aug 89	April 1990	102

16 SUPPLEMENTARY NOTATION
N/A

17 COSATI CODES			18 SUBJECT TERMS (Continue on reverse if necessary and identify by block number)
FIELD	GROUP	SUB-GROUP	Phase Only Filters; Optical Data Processing; Correlators; Binary Phase Only Filters
09	04		

19 ABSTRACT (Continue on reverse if necessary and identify by block number)

This report summarizes the results obtained during Contract No. F19628-88-K-0018 entitled "Optimal Phase-only Filters). This research was focused on Phase-only Filters (POFs) and Binary Phase-only Filters (BPOFs).

We prove in this report that the conventional POF introduced originally by Horner and Gianino is indeed the best among all POFs from the viewpoint of maximizing the Signal-to-Noise Ratio (SNR). We also illustrate the importance of selecting the optimal support function for the POF and show with the help of example images that output SNR can be improved considerably (by about 5 dB) by using optimal POFs (OPOFs). This report describes an efficient algorithm for designing OPOFs.

Because of their suitability for binary Spatial Light Modulators (SLMs) such as the Magneto Optic SLM (MOSLM), binary POFs (BPOFs) are of (Continued on Reverse)

20 DISTRIBUTION/AVAILABILITY OF ABSTRACT	21 ABSTRACT SECURITY CLASSIFICATION	
☐ UNCLASSIFIED/UNLIMITED ☒ SAME AS RPT ☐ DTIC USERS	UNCLASSIFIED	
22a NAME OF RESPONSIBLE INDIVIDUAL Joseph Horner	22b TELEPHONE (Include Area Code) (617) 377-3841	22c OFFICE SYMBOL RADC (ESO)

DD Form 1473, JUN 86 Previous editions are obsolete. SECURITY CLASSIFICATION OF THIS PAGE

UNCLASSIFIED

Block 19 Continued:

much interest. In this report, we introduce the optimal BPOF (OBPOF) and present efficient algorithms for designing OBPOFs. Several simulation results based on the use of 32 X 32 images are included to verify the performance of OBPOFs.

Abstract

This report summarizes the results obtained during the contract No. F 19628-88-K-0018 entitled "Optimal Phase-only Filters". This research was focused on Phase-only Filters (POFs) and Binary Phase-only Filters (BPOFs).

We prove in this report that the conventional POF introduced originally by Horner and Gianino is indeed the best among all POFs from the viewpoint of maximizing the Signal-to-Noise Ratio (SNR). We also illustrate the importance of selecting the optimal support function for the POF and show with the help of example images that output SNR can be improved considerably (by about 5 dB) by using optimal POFs (OPOFs). This report describes an efficient algorithm for designing OPOFs.

Because of their suitability for binary Spatial Light Modulators (SLMs) such as the Magneto Optic SLM (MOSLM), binary POFs (BPOFs) are of much interest. In this report, we introduce the optimal BPOF (OBPOF) and present efficient algorithms for designing OBPOFs. Several simulation results based on the use of 32×32 images are included to verify the performance of OBPOFs.

Chapter 1

Introduction

1.1. Motivation

While the original idea of optical matched spatial filters was introduced by VanderLugt[1] more than twenty five years ago, they have not become practicable for the three main reasons given below.

- The filters required for matched spatial filtering are complex valued and thus cannot be easily accommodated on currently available Spatial Light Modulators (SLMs).
- The matched spatial filters (MSFs) are overly sensitive to small changes in the reference image and thus their performance deteriorates significantly in the presence of image distortions.
- The light throughput efficiency of MSFs is low because the filter frequency response is less than one for many frequencies.

Several ideas have been proposed to alleviate the above problems. Horner and Gianino[2] suggested the use of Phase-only Filters (POFs) to improve the light efficiency of correlation filters. Similarly, use of Binary POFs (BPOFs)[3, 4] is proposed for easy implementation on real-time SLMs such as the Magneto Optic SLM (MOSLM). While the original ideas of POFs and BPOFs have been tested using computer simulations and optical experiments, not much attention has been paid to deriving optimal POFs and optimal BPOFs. This research report summarizes the results obtained for designing optimal POFs and BPOFs under the contract numbered F 19628-88-K-0018 and entitled "optimal phase-only filters".

1.2. Research Contributions

Following important results were established during this research contract. More details regarding these results are available in chapters 2 and 3.

- We provided a theoretical proof that the conventional POF introduced by Horner and Gianino is indeed the optimal (from the viewpoint of maximizing the Signal-to-Noise Ratio (SNR)) among all unit-modulus filters.

- We proved that the SNR obtained from the conventional POF can be further improved by selecting the support function of the POF appropriately. The POFs with support functions chosen to maximize the output SNR are termed the Optimal POFs (OPOFs).

- We derived an efficient algorithm for selecting the support function of the OPOF. We have developed the appropriate software and made several refinements to the basic algorithm to improve its efficiency.

- We carried out extensive simulations to illustrate the SNR improvements obtained by using OPOFs. Using 32×32 images of a tank, we observe an SNR improvement of about 3.5 dB.

- We carried out extensive simulations to quantify the distortion sensitivity of the OPOFs. It is observed that OPOFs are less sensitive to distortions than the conventional POFs. Similarly, POFs are more light efficient that OPOFs.

- We developed a method for designing the optimal support function when the output correlation detector is noisy. It is shown that for low-noise detectors, the support function will be the same as that of the OPOFs. However, when the detectors are noisy, the filter support function should be opened up as wide as possible.

- We showed that the results proved by Farn and Goodman[5] for designing optimal binary POFs are incomplete and that they missed a subtle point. We completed this proof and showed that the selection of an appropriate support function can improve the SNR of the BPOF. These are termed Optimal BPOF (OBPOFs).

- We developed a very efficient method for deriving the support function for the OBPOF. This method searches over all possible Threshold Line Angles (TLAs) to design the optimal support function.

- We have carried out extensive simulations to characterize the OBPOF and have observed about 5 dB improvement in SNR compared to the BPOF.

1.3. Organization

The remainder of this report is organized as follows. In chapter 2, we provide the proofs and results concerning Phase-only Filters. After a brief introduction is Sect. 2.1, we provide the necessary background in Sect. 2.2. The concept of OPOF is introduced in Sect. 2.3 along with a few illustrative examples. Then we introduce an efficient algorithm for designing OPOFs in Sect. 2.4. In Sect. 2.5, we present an even faster algorithm that designs a slightly sub-optimal POF. The distortion sensitivity of the OPOFs is then evaluated numerically in Sect. 2.6. The OPOFs are extended to the 2-class problem in Sect. 2.7 and the effects of detector limitations are included in Sect. 2.8.

A similar format is used for the BPOF discussion in Chapter 3. An efficient algorithm for designing OBPOFs is presented in Sect. 3.2 and some numerical results obtained using it are presented in Sect. 3.3. A slightly sub-optimal, but very efficient algorithm is presented in Sect. 3.4. Then, in Sect. 3.5, we unify the OPOF and OBPOF algorithms. Sect. 3.6 addresses the issue of bifurcation that seems to appear in BPOFs. Finally, the distortion sensitivity of OBPOFs is explored in Sect. 3.7.

Chapter 2

Phase-only Filters

2.1. Introduction

Since the introduction of the frequency plane correlator by Vander Lugt[1], matched spatial filters (MSFs) have been very popular in optical pattern recognition. The MSFs yield the highest possible Signal-to-Noise Ratio (SNR) when detecting a known signal/image corrupted by additive white noise. The use of the MSFs in optical processors requires that we have the ability to represent both the magnitude and the phase of the complex-valued filter plane function. However, several spatial light modulators (SLMs)[6, 7, 8] of current interest can function in a *phase-only* mode and thus the filters used must be phase-only.

Recently, Horner and Gianino[2, 9] introduced the notion of using the phase-only version of the conventional MSF by setting the filter magnitude to 1 for all frequencies. Such a filter will be referred to as the Phase-Only Filter (POF). Hence, the POF yields *continuous* variations in its phase function only. Even though this is not directly compatible with SLMs such as the MOSLM[6], operating in a *discrete* phase-only mode, the POF was still considered as a step towards achieving matched filtering using SLMs, and has triggered considerable amount of research in the area of phase-only filtering. In fact, many researchers have proposed to bridge this gap by a simple binarization of the POF to obtain Binary Phase-Only Filters (BPOFs)[10, 3, 11]. Yet, despite this increased interest in the use of POFs, we are not aware of any research that theoretically *investigates* the optimality of the conventional POF[2]. In this chapter we fill this void and establish

methods of *optimally* designing POFs. We provide a formal proof that, with proper selection of the filter *support* (i.e., the region consisting of all frequencies at which the filter's magnitude is non-zero), the conventional POF does indeed yield the highest SNR. The resulting filter (with the corresponding support) will be termed the Optimal Phase-Only Filter (OPOF). We also illustrate and quantify the improvement in SNR (resulting from the use of OPOFs) with the help of both analytical examples as well as realistic image examples. We analyze the various characteristics of the optimal support for OPOFs, and provide an efficient algorithm for its design in addition to a very efficient sub-optimal technique. The sensitivity of POFs and OPOFs to input distortion is also examined, as well as the effect of detector noise on the design of OPOFs. We must emphasize that this chapter is intended for the detection of *known* signals/images in noise whereas some of the other approaches presented in the literature[12, 13, 14, 15] are aimed at distortion-invariant pattern recognition with phase-only filters.

The remainder of this chapter is organized as follows. In Section 2, we present some background material related to the detection problem and matched filtering. In section 3, we provide the derivation of the OPOF along with some analytical examples that illustrate the resulting improvement in SNR. In section 4, we develop an efficient algorithm for numerically solving for the support of OPOFs in the presence of white noise. We illustrate the algorithm using two realistic images (tank and pliers). Section 5 is used to present a very efficient sub-optimal algorithm for the design of OPOFs with white noise. While this algorithm causes a very small loss in SNR (of the order of 10^{-4} dB), the speed up factor it leads to is substantial (about two orders of magnitude). In Section 6, we investigate the distortion sensitivity of OPOFs and POFs to input distortion with the help of computer simulations. Section 7 deals with a two-class detection problem. Section 8 is devoted to analyzing the effect of the detector noise on the design of OPOFs. Finally, Section 9 summarizes our results.

2.2. Background

2.2.1. Matched Filtering

We start with the well-known derivation of the optimality of the matched filter to set up some of the notation needed for the following sections. In a *detection* problem, the observed signal $r(x)$ is given by

$$r(x) = s(x) + n(x) \ , \tag{2.1}$$

where $s(x)$ is the known reference signal and $n(x)$ represents additive stationary noise with zero mean and power spectral density $P_n(f)$. The presence of the reference signal is detected by letting $r(x)$ be the input to a linear, time-invariant system with impulse response $h(x)$ (or equivalently with transfer function $H(f)$) and sampling the corresponding output (without loss of generality) at $x = 0$. If this sampled output value exceeds a pre-determined threshold, then the decision that "Signal $s(x)$ is present in $r(x)$" is made and if the sampled output value falls below that threshold, it is decided that "Signal $s(x)$ is not present in $r(x)$".

To determine the $H(f)$ that yields the best performance, the following Signal-to-Noise Ratio (SNR) measure is usually maximized.

$$\text{SNR} = \frac{| \int S(f) \ H(f) df \ |^2}{\int P_n(f) \ | \ H(f) \ |^2 \ df} \ , \tag{2.2}$$

where $S(f)$ is the Fourier Transform (FT) of $s(x)$ and the limits of integration are from $-\infty$ to $+\infty$. The numerator of Eq. (2.2) denotes the square of the modulus of the average output value when $s(x)$ is present whereas the denominator is the variance in the sampled output. Thus, better detection performance is expected with filters yielding higher SNR values. This SNR is the measure used in the derivation of the classical matched filter[16]

and is *different* from another useful measure known as the Peak-to-Sidelobe Ratio (PSR). The PSR is defined as the ratio of the square of the output peak value (presumably located at $x = 0$) to the variance of the output function away from this peak. Thus, SNR is a measure of how well a filter performs in the presence of additive noise whereas the PSR is a measure of how sharp the output peak from that filter is. Unless otherwise stated, we consider the SNR as our performance criterion as is the practice in classical matched filter derivation.

To find the filter $H(f)$ yielding the highest SNR, we apply Cauchy-Schwartz inequality to the numerator of Eq. (2.2) to obtain the following.

$$\text{SNR} = \frac{| \int [\, \sqrt{P_n(f)}\, H(f)\,]\, [\, \frac{S(f)}{\sqrt{P_n(f)}}] \, df \,|^2}{\int P_n(f)\, |H(f)|^2 df}$$

$$\leq \frac{[\, \int P_n(f)\, |\, H(f)\, |^2 df\,]\, [\int \frac{|\, S(f)\, |^2}{P_n(f)}\, df]}{\int P_n(f)\, |H(f)|^2 df}$$

$$= \int \frac{|\, S(f)\, |^2}{P_n(f)}\, df \;=\; \text{SNR}_{\text{MSF}} \tag{2.3}$$

with equality occurring if and only if

$$H(f) = \alpha \frac{S^*(f)}{P_n(f)}\,, \tag{2.4}$$

where α is an arbitrary complex constant that does not affect the resulting SNR.

For white noise, $P_n(f)$ is a constant and $H(f) = S^*(f)$ or $h(x) = s(-x)$ and the filter output turns out to be the cross-correlation of the received signal $r(x)$ with the reference signal $s(x)$. For colored noise, cross-correlation is *not* equivalent to optimal filtering. It is worth emphasizing that *no* other filter (phase-only filter or any other) can yield a higher SNR than $\mathrm{SNR}_{\mathrm{MSF}}$. The optimum filter of Eq. (2.4) can also be written (assuming $\alpha = 1$) as

$$H(f) = \frac{|S(f)|}{P_n(f)} \, e^{-j\Phi_s(f)} \quad , \tag{2.5}$$

where $|S(f)|$ is the magnitude of $S(f)$ and $\Phi_s(f)$ its phase function. Thus the optimal filter is in general *complex*.

2.2.2. Conventional POF

The concept of phase-only filters (POFs) in optical correlators was introduced in 1984 by Horner and Gianino[2]. In order to improve the light throughput of the optical correlator[i], they suggested that the magnitude in Eq. (2.5) be set to 1 at all frequencies. The resulting phase-only filter (POF) is then

$$H_{\mathrm{POF}} = \mathrm{e}^{-j\Phi_s(f)} . \tag{2.6}$$

The use of POF was somewhat justified based on the observation[17] that the phase of the Fourier transform of an image seemed to retain more information than its magnitude. This POF has been tested with the help of some images and was seen[9, 18] to have the following properties:

- POF yields *sharper* correlation peaks than the classical matched filter.

---

[i]Even though improving the light throughput has been one of the motivations behind the introduction of POFs, taking the complex matched filter one step closer to its real-time implementation using the recently developed SLMs is probably an implicitly stronger motivation.

- POF has higher light efficiency (in fact, 100%).
- POF results in higher peak-to-sidelobe ratios than the classical matched filter.

While the use of POFs for optical pattern recognition has been justified with the help of several examples, the approaches presented in the literature so far (except for a few[15]) are more or less "after-thoughts", i.e., these POFs are obtained by determining an optimal filter and then setting its magnitude to a constant arbitrarily. Strictly speaking, there is no *a priori* reason why the phase of the Optimal POF should be set equal to the phase of the matched filter. Furthermore, the bandwidth of the POF is usually allowed to be arbitrarily large (usually only limited by the optical system aperture). Even though this yields sharp correlation peaks, it also allows all the noise present in the input to pass through unattenuated. Indeed, the POF can be viewed as the cascade of the matched filter with a second filter whose frequency response equals $\frac{P_n(f)}{|S(f)|}$. Since $|S(f)|$ is usually small for high frequencies, the second filter actually turns out to be a *high pass* filter. This implicit high-pass filtering effect[19] seems to be the main reason for one of the problems associated with POFs, namely sensitivity to input noise. Hence, there is a definite need for proper support selection when dealing with POFs. In the next section, we will describe a different approach where an optimal phase-only filter will be designed *starting* with the constraint that it is a phase-only filter.

2.3. Optimal Phase-only Filters

2.3.1. Derivation of OPOF

We now derive the optimal phase-only filter (OPOF) that maximizes the SNR in Eq. (2.2). Towards this end, let us assume that $S(f)$ is zero for f not in region $\mathcal{S}$. We start with the constraint that the desired filter $H(f)$ is of the following form.

$$H(f) = \mathrm{I}_{\mathcal{R}}(f)\, e^{j\Phi(f)} \ , \tag{2.7}$$

where $\Phi(f)$ is the phase of the POF (not necessarily equal to $-\Phi_s(f)$) and where $I_{\mathcal{R}}(f)$ denotes the *indicator function* of the region $\mathcal{R}$ (support) defined as

$$I_{\mathcal{R}}(f) = \begin{cases} 1 & \text{if } f \in \mathcal{R} \\ 0 & \text{otherwise} \end{cases} . \tag{2.8}$$

Using Eq. (2.7), the SNR in Eq. (2.2) can be rewritten as

$$\text{SNR}_{\text{POF}} = \frac{| \int_{\mathcal{R}} S(f)\, e^{j\Phi(f)}\, df\, |^2}{\int_{\mathcal{R}} P_n(f)\, df} . \tag{2.9}$$

We can find an upper bound to the SNR in Eq. (2.9) as below:

$$\begin{aligned} \text{SNR}_{\text{POF}} &= \frac{| \int_{\mathcal{R}} |S(f)|\, e^{j(\Phi_s(f)+\Phi(f))}\, df\, |^2}{\int_{\mathcal{R}} P_n(f) df} \\ &\leq \frac{[\int_{\mathcal{R}} |S(f)|\, |\, e^{j(\Phi_s(f)+\Phi(f))}\, |\, df\,]^2}{\int_{\mathcal{R}} P_n(f) df} \\ &= \frac{[\int_{\mathcal{R}} |\, S(f)|\, df\,]^2}{\int_{\mathcal{R}} P_n(f) df} . \end{aligned} \tag{2.10}$$

Thus for a given support $\mathcal{R}$, the maximum SNR obtainable from *any* phase-only filter is given by

$$\text{SNR}_{\text{OPOF}} = \frac{[\int_{\mathcal{R}} |S(f)|df]^2}{\int_{\mathcal{R}} P_n(f)df} . \tag{2.11}$$

From the first line in Eq. (2.10), we see that the phase-only filter that achieves the optimal SNR in Eq. (2.11) has its phase given by

$$\Phi(f) = -\Phi_s(f) + \theta , \tag{2.12}$$

where θ is any constant. We will assume from now on (without any loss of generality) that $\theta = 0$. Thus, for a given $\mathcal{R}$, the conventional phase-only filter $e^{-j\Phi_s(f)}$ *does* indeed give the highest possible SNR.

Now the SNR in Eq. (2.11) can be further optimized by properly selecting the support $\mathcal{R}$. Unfortunately, Finding the optimal support $\mathcal{R}_{opt}$ is in general a fairly difficult task. Nevertheless, some characterizations of $\mathcal{R}_{opt}$ can be provided. This will be the object of focus of the next section.

2.3.2. Optimal Support Characterization

First, for OPOF, we must have

$$\mathcal{R}_{opt} \subseteq \mathcal{S} , \tag{2.13}$$

otherwise, we can easily see from Eq. (2.2) that the denominator will increase with no increase in the numerator. Before we present two other results, we list some useful definitions.

- A region $\mathcal{R}^s$ is said to be *symmetric* iff

$$\forall\ f \in \mathcal{R}^s ,\ \ -f \in \mathcal{R}^s . \tag{2.14}$$

- A region $\mathcal{R}^a$ is said to be *anti-symmetric* iff

$$\forall\, f \in \mathcal{R}^a, \quad -f \notin \mathcal{R}^a \,. \tag{2.15}$$

- We define the *mirror image* of an anti-symmetric region $\mathcal{R}^a$ (denoted $\mathcal{R}^{a-}$) by

$$\mathcal{R}^{a-} = \{ f\colon\ -f \in \mathcal{R}^a \} \,. \tag{2.16}$$

Note that $\mathcal{R}^{a-}$ is itself anti-symmetric.

- Any region $\mathcal{R}$ can be *partitioned* as

$$\mathcal{R} = \mathcal{R}^s \cup \mathcal{R}^a \,, \tag{2.17}$$

where, $\mathcal{R}^s$ and $\mathcal{R}^a$ (disjoint) are given by

$$\mathcal{R}^s = \{ f \in \mathcal{R} : \ -f \in \mathcal{R} \} \,, \tag{2.18}$$

and

$$\mathcal{R}^a = \mathcal{R} \setminus \mathcal{R}^s \,. \tag{2.19}$$

In the above, the symbol "\" denotes the *set difference* operation.

Proposition 1: $\mathcal{R}_{opt}$ is *even symmetric* for real reference images.

Proof: Recall that we want to find $\mathcal{R}$ that maximizes the SNR in Eq. (2.11). Then, the optimal support $\mathcal{R}_{opt}$ can be decomposed as

$$\mathcal{R}_{opt} = \mathcal{R}^s_{opt} \cup \mathcal{R}^a_{opt} \,. \tag{2.20}$$

Let us now assume that

$$\mathcal{R}^a_{opt} \neq \emptyset \,. \tag{2.21}$$

There are two cases:

1. $\mathcal{R}^s_{opt} = \emptyset$. In this case, it is not difficult to see that by using $\mathcal{R}' = \mathcal{R}^a_{opt} \cup \mathcal{R}^{a-}_{opt}$ we double the SNR, i.e.,

$$SNR(\mathcal{R}') = 2\,SNR(\mathcal{R}_{opt}). \qquad \underline{\text{Absurd}}\,. \tag{2.22}$$

In the above, we made use of the fact that

$$|S(-f)| = |S(f)|\ , \tag{2.23}$$

which is a direct consequence of the assumption that $s(x)$ is real.

2. $\mathcal{R}^{s}_{opt} \neq \emptyset$. The objective now is to show that by using

$$\mathcal{R}' = \mathcal{R}_{opt} \cup \mathcal{R}^{a-}_{opt}\ , \tag{2.24}$$

we get higher SNR, resulting in an absurd situation. Let

$$\alpha = \int_{\mathcal{R}^{s}_{opt}} |S(f)|\,df\ , \tag{2.25}$$

$$\beta = \int_{\mathcal{R}^{a}_{opt}} |S(f)|\,df\ , \tag{2.26}$$

$$\eta = \int_{\mathcal{R}^{s}_{opt}} P_n(f)\,df\ , \tag{2.27}$$

$$\xi = \int_{\mathcal{R}^{a}_{opt}} P_n(f)\,df\ . \tag{2.28}$$

Using Eqs. (2.25)-(2.28), Eq. (2.24), and Eq. (2.23) in Eq. (2.11), we get

$$\begin{aligned} &SNR(\mathcal{R}_{opt}) - SNR(\mathcal{R}') \\ &= \frac{(\alpha+\beta)^2}{\eta+\xi} - \frac{(\alpha+2\beta)^2}{\eta+2\xi} \\ &= \frac{\alpha^2\xi - \beta^2\eta - 2\alpha\beta\eta - 2\beta^2(\eta+\xi)}{(\eta+\xi)(\eta+2\xi)} < 0\ . \end{aligned} \tag{2.29}$$

$\underline{\text{Absurd}}$.

The above strict inequality comes from the fact that

$$SNR(\mathcal{R}^s_{opt}) \leq SNR(\mathcal{R}_{opt})$$

$$\Rightarrow \frac{\alpha^2}{\eta} \leq \frac{(\alpha+\beta)^2}{\eta+\xi}$$

$$\Rightarrow \alpha^2\xi - \beta^2\eta - 2\alpha\beta\eta \leq 0 , \tag{2.30}$$

and the fact that[ii]

$$\beta^2(\eta+\xi) > 0 . \tag{2.31}$$

Hence, in conclusion, our assumption in Eq. (2.21) cannot be true and $\mathcal{R}_{opt}$ must be symmetric •

Proposition 2: For white noise,

$$\mathcal{R}_{opt} = \{ f : |S(f)| > \epsilon_o \} , \tag{2.32}$$

where, ϵ_o is a positive constant (to be determined) that depends on $|S(f)|$ and the white noise level.

Proof: Assuming white noise, the above result follows directly from the observation that to maximize the SNR, we want the frequencies with the largest magnitudes to be included in the passband first. This is exactly achieved by comparing $|S(f)|$ to some threshold and rejecting all those frequencies with magnitudes below the threshold[iii]. However, there is a subtle issue that needs to be addressed. Let us denote by S_ϵ the set

[ii]Note that β is non-zero from the assumption given in Eq. (2.21).

[iii]For example, for all signal spectra for which the OPOF turns out to be a low pass filter (examples of such spectra will follow in next sections) it can easily be seen that the optimal passband is given by the set of all those frequencies at which the magnitude of $S(f)$ is greater than ϵ_o given by

$$\epsilon_o = |S(W_h)| , \tag{2.33}$$

where W_h is the optimal cut-off frequency of the OPOF. Unfortunately, no other information can be given about ϵ_o, and in general, it depends on $S(f)$ and the white noise level. Actually, Eq. (2.33) points out that finding the optimal threshold ϵ_o in general involves the same level of difficulty as finding the optimal cut-off frequency (namely solving a transcendental equation, as will be seen shortly).

$$S_\epsilon = \{ f : |S(f)| > \epsilon \} , \tag{2.34}$$

then the Lebesgue measure of S_ϵ ($\mu(S_\epsilon)$) as a function of ϵ shows a discontinuity of the first kind (i.e., a "jump") whenever $|S(f)|$ is constant over a region of non-zero measure. This is illustrated by the example in Figs. 2-1 and 2-2. This could cause problems in the sense that if one of the optimal cut-off frequencies (there could be more than one for the case where the OPOF is a multi pass filter) lies in the *interior* of a region (with non-zero measure) over which $|S(f)|$ is constant, then the optimal support cannot take the form given in Eq. (2.32). Another way of stating this difficulty is that the sets in Eq. (2.32) cannot "resolve" those non-zero measure regions over which $|S(f)|$ is constant.

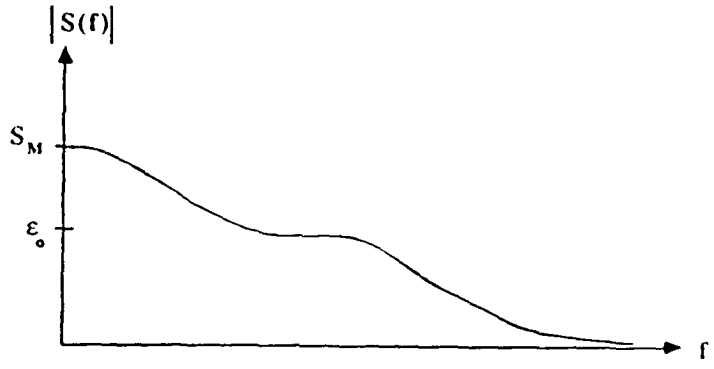

Figure 2-1: Hypothetical signal spectrum.

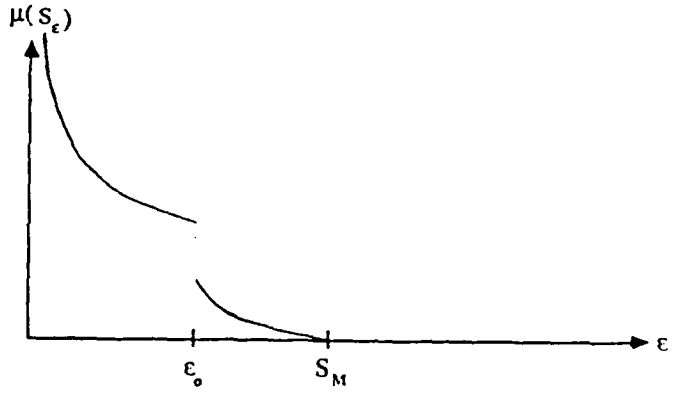

Figure 2-2: Lebesgue measure of S_ϵ for above spectrum.

It turns out that the above case is forbidden, i.e., no optimal cut-off frequency can be in the interior of such a region. This fact can be easily proved.

It can be checked that by enlarging the cut-off frequency by an infinitesimal increment, we get higher SNR. A similar proof will be given in a forthcoming section •

While the above results somewhat characterize $\mathcal{R}_{opt}$, they remain of academic importance only, since they do not explicitly lead to the optimal region. Later on, we will introduce numerical techniques based on this characterization to solve this problem.

2.3.3. Analytical Examples

To analytically investigate the effect of proper support selection on the performance of the system, we need to make some simplifying assumptions. First, we will assume that most of the energy of the reference signal lies in the low frequency region of the spectrum. Second, we will assume the power spectral density of the noise to be much wider than the spectrum of the reference. With these assumptions, the OPOF turns out to be a low pass filter (i.e., the optimal region $\mathcal{R}_{opt}$ is a low frequency region). Hence the OPOF is given by

$$H(f) = \begin{cases} e^{-j\Phi_s(f)} & \text{for } |f| \leq W_h \\ 0 & \text{otherwise} \end{cases}, \tag{2.35}$$

where W_h is the cut-off frequency of the OPOF. Then, the SNR expression given in Eq. (2.11) can be written explicitly as a function of W_h as

$$\text{SNR}_{\text{OPOF}} = \frac{2\left[\int_0^{W_h} |S(f)|df\right]^2}{\int_0^{W_h} P_n(f)df}, \tag{2.36}$$

Where we used the fact that for real signals both $|S(f)|$ and $P_n(f)$ have even symmetry.

To find the best choice for W_h, we set the derivative of $\mathrm{SNR}_{\mathrm{OPOF}}$ in Eq. (2.36) with respect to W_h to zero. Thus W_h is the solution to the following equation.

$$[2\int_0^{W_h} P_n(f)\,df]\,|S(W_h)| = [\int_0^{W_h} |S(f)|\,df]\,P_n(W_h)\,. \tag{2.37}$$

To solve Eq. (2.37), let us define the following new functions.

$$P_n'(W_h) = \frac{2}{P_n(W_h)}\int_0^{W_h} P_n(f)\,df\,, \tag{2.38}$$

and

$$S'(W_h) = \frac{1}{|\,S(W_h)\,|}\int_0^{W_h} |S(f)|\,df \quad . \tag{2.39}$$

Then the optimum W_h can be obtained as the solution to the following equation.

$$S'(W_h) = P_n'(W_h) \quad . \tag{2.40}$$

From a geometrical point of view, this can be done finding the intersection of the curves $S'(W_h)$ and $P_n'(W_h)$. In case this equation cannot be solved explicitly (i.e., the functions $S'(W_h)$ and $P_n'(W_h)$ do not intersect), we must graph the $\mathrm{SNR}_{\mathrm{OPOF}}$ in Eq. (2.36) as a function of W_h and choose the W_h yielding the maximum $\mathrm{SNR}_{\mathrm{OPOF}}$. We now present a few examples to illustrate the necessity of proper bandwidth selection. Let the noise be white noise with a power spectral density of N_0.

2.3.3.1. Triangular Signal Spectrum

Here we assume that the magnitude of the signal FT is as below.

$$| S(f) | = \begin{cases} (1-\frac{|f|}{W_s}) \text{ for } |f| \leq W_s \\ 0 \quad \text{otherwise} \end{cases} . \tag{2.41}$$

Substituting Eq. (2.41) in Eq. (2.36), we see that $\text{SNR}_{\text{OPOF}}(W_h)$ is given by

$$\text{SNR}_{\text{OPOF}}(W_h) = \frac{2W_h}{N_0}(1 - \frac{W_h}{2W_s})^2 \quad . \tag{2.42}$$

It is easy to verify that the SNR_{OPOF} in Eq. (2.42) can be maximized by choosing

$$W_h = \frac{2}{3} W_s \quad . \tag{2.43}$$

The resulting maximum SNR from an optimal phase-only filter is given by

$$\text{SNR}_{\text{OPOF}} = \frac{16}{27} \frac{W_s}{N_0} \quad . \tag{2.44}$$

If we use the full signal bandwidth W_s for the filter (as is done for the conventional POF), the resulting SNR is given by

$$\text{SNR}_{\text{POF}} = \frac{2W_s}{N_0}(1 - \frac{W_s}{2W_s})^2 = \frac{W_s}{2N_0} \quad . \tag{2.45}$$

It is obvious from Eq. (2.44) and Eq. (2.45) that the conventional POF yields smaller SNR values than our optimal POF. Of course, both these SNRs are lower than that obtained from the classical matched filter.

$$\text{SNR}_{\text{MSF}} = \frac{2}{N_0}\int_0^{W_s}(1-\frac{f}{W_s})^2 df = \frac{2W_s}{3N_0} \quad . \tag{2.46}$$

This example clearly illustrates that

$$\text{SNR}_{\text{POF}} \leq \text{SNR}_{\text{OPOF}} \leq \text{SNR}_{\text{MSF}} \quad . \tag{2.47}$$

More exactly, the conventional POF yields a SNR 1.25 dB lower than that of the classical MF whereas our OPOF yields a SNR only 0.51 dB lower than that of the classical matched filter.

2.3.3.2. Cosinusoidal Signal Spectrum

In this example, the magnitude of the signal FT is given by

$$|S(f)| = \begin{cases} \cos\left(\frac{\pi f}{2W_s}\right) & \text{for } |f| \leq W_s \\ 0 & \text{otherwise} \end{cases} \quad . \tag{2.48}$$

Substituting Eq. (2.48) in Eq. (2.40) and simplifying, we obtain the following transcendental equation in W_h.

$$\frac{W_h}{W_s} = \frac{1}{\pi}\tan\left[\frac{\pi}{2}\frac{W_h}{W_s}\right] \quad . \tag{2.49}$$

While this transcendental equation has many possible solutions, we require that $0 < \frac{W_h}{W_s} \leq 1$. By numerically solving Eq. (2.49), we determined that the solution is approximately given by

$$W_h = 0.742\, W_s \quad . \tag{2.50}$$

Substituting Eq. (2.50) in Eq. (2.36), we found that $\mathrm{SNR}_{\mathrm{OPOF}}$ equals $0.9226\ (\frac{W_s}{N_0})$. The $\mathrm{SNR}_{\mathrm{MSF}}$ can be shown to be $(\frac{W_s}{N_0})$. The conventional POF uses the full bandwidth $W_h = W_s$ and the resulting SNR is $(\frac{8}{\pi^2})\ (\frac{W_s}{N_0})$. Thus, the conventional POF has a SNR 0.912 dB below that of the classical matched filter whereas the OPOF yields a SNR only 0.35 dB below that of the classical matched filter.

2.3.3.3. Sinc Signal Spectrum

The previous two examples involved only relatively small improvements in the SNRs. In this subsection, we show a more dramatic example. The magnitude of the signal FT is given by[iv]

$$| S(f) | = | \mathrm{Sinc}\ (fT) | \ , \tag{2.51}$$

where T is a known constant. Such a magnitude Fourier transform occurs when the signal is a rectangle function that is zero outside $-T/2 \leq x \leq T/2$. The $\mathrm{SNR}_{\mathrm{MSF}}$ for this signal can be easily shown to be

$$\mathrm{SNR}_{\mathrm{MSF}} = \frac{1}{N_0} \int_{-\infty}^{\infty} \mathrm{Sinc}^2(fT)\, df = \frac{1}{N_0 T} \ . \tag{2.52}$$

For the conventional POF, the $| H(f) |$ is 1 for all frequencies because $|S(f)|$ has infinite bandwidth (even though, in practice, any filter will be band limited) and from Eq. (9), we obtain

[iv] Here, we define $\mathrm{Sinc}(x)$ as $\frac{\sin(\pi x)}{\pi x}$.

$$\text{SNR}_{\text{POF}} = \frac{(\int_{-\infty}^{\infty} |\,\text{Sinc}\,(fT)\,|\,df)^2}{\int_{-\infty}^{\infty} N_0\,df} = 0\,. \tag{2.53}$$

The W_h defining the OPOF can be obtained by evaluating SNR_{OPOF} in Eq. (2.36) as a function of W_h and finding the W_h that maximizes it. This evaluation was done numerically and after some approximations, it was found that $W_h = 0.6855/T$ yields the highest output SNR. For this choice of W_h, the resulting SNR_{OPOF} is seen to be

$$\text{SNR}_{\text{OPOF}} = \frac{2[\int_0^{W_h} |\,\text{Sinc}\,(fT)|df\,]^2}{N_0 \int_0^{W_h} df} = \frac{0.8245}{N_0 T}\,. \tag{2.54}$$

In the above SNR evaluation as well as in the solution of W_h, we made use of the following series expansion[20]

$$\int_0^{W_h} \text{Sinc}\,(Tf)\,df = \frac{1}{\pi T}\sum_{i=1}^{\infty} \frac{(-1)^{i+1}(\pi T W_h)^{2i-1}}{(2i-1)\,(2i-1)!}\,. \tag{2.55}$$

Comparing the SNRs in Eqs. (2.52) and (2.54), we see that the OPOF yields an SNR that is only 0.838 dB below that of the matched filter. On the other hand, the conventional POF is overwhelmed by the white noise because of its all-pass nature and yields a zero SNR.

We realize that it is unwise to allow any POF to have an infinite bandwidth. However, this example clearly brings out two points. Firstly, it shows that proper selection of POF bandwidth is essential for obtaining a reasonable SNR. Secondly, it shows that one is trading off SNR against sharpness of correlation peaks. For example,

when the conventional POF has infinite bandwidth, it will yield the sharpest correlation peaks, but with zero SNRs.

2.3.4. Comment on Zero-mean Noise Assumption

In our formulation of the detection problem, we have made the assumption that the noise corrupting the input has zero mean. Even though this assumption may be valid in a communication theory context, it may not be so in an optical pattern recognition context, because the imaging devices used to display the input are usually intensity sensitive. As a result, the additive noise $n(x)$ we deal with in an optical correlator has a positive mean m_n. If m_n is known *a priori*, then its contribution to the filter output (at the origin) is a known *deterministic* value given by

$$y_{m_n}(0) = m_n H(0) \ , \tag{2.56}$$

where, $H(0)$ is the transfer function of the filter evaluated at the origin. Hence, if we subtract this value from the total output at the origin, we would cancel the effect of the non-zero mean of the noise. Thus, if we redefine the SNR as

$$\text{SNR} = \frac{| E\{ [y(0) - m_n H(0)] / \text{signal present} \} |^2}{var\{y(0)\}} \ , \tag{2.57}$$

we get exactly the expression in Eq. (2.2), and we can proceed as before. In Eq. (2.57), $y(0)$ denotes the output value at the origin, $E\{a/c\}$ denotes the expected value of a conditioned on c, and $var\{a\}$ denotes the variance of a.

If, however, m_n is not known *a priori*, we cannot cancel its effect by a simple subtraction. Instead, let us rewrite $n(x)$ as the sum of two components: A realization from a zero mean random process $n_o(x)$ and the mean value m_n, i.e.,

$$n(x) = n_o(x) + m_n \ . \tag{2.58}$$

Similarly, we rewrite $s(x)$ as a zero-mean signal added to a positive DC bias, i.e.,

$$s(x) = s_o(x) + m_s \ . \tag{2.59}$$

We can see from Eq. (2.58) that

$$P_n(f) = P_{n_o}(f) + m_n^2 \, \delta(f) \ , \tag{2.60}$$

where, $\delta(f)$ is a delta function. Hence, the SNR expression is given by

$$\begin{aligned} \text{SNR} &= \frac{|\, E\{y(0)/ \text{ signal present } \}|^2}{var\{y(0)\}} \\ &= \frac{|\int_{-\infty}^{\infty} S_o(f)H(f)\,df \ + \ +(m_n + m_s)H(0)\,|^2}{\int_{-\infty}^{\infty} P_{n_o}(f)\,|H(f)|^2\,df \ + \ m_n^2|H(0)|^2} \ . \end{aligned} \tag{2.61}$$

If we assume

$$H(0) = 0 \ , \tag{2.62}$$

then the SNR expression in Eq. (2.61) reduces to Eq. (2.2) with $S_o(f)$ and $P_{n_o}(f)$ replacing $S(f)$ and $P_n(f)$, respectively. Eq. (2.62) expresses the well known practice of introducing a DC block at the frequency plane of an optical correlator. Notice that the filter that optimizes Eq. (2.61) subject to the condition given in Eq. (2.62), is given by

$$H_{opt}(f) = \alpha \frac{S_o^*(f)}{P_{n_o}(f)} \tag{2.63}$$

(the condition that $H(0) = 0$ is satisfied from the fact that $S_o(0) = 0$). Once again, we observe from Eq. (2.63) that for the case of white noise, optimal (among all filters with zero DC value) filtering is equivalent to a "slightly modified" correlation operation. Hence, the fact that the additive white noise has a non-zero mean does not make the optical correlator lose its optimality, since we just argued that a correlator with a DC block is the best among all filters with DC blocks.

In conclusion, the non-zero mean of the input noise can, without loss of generality, be ignored by a small modification of the output value. This modification could be performed by a direct subtraction from the output of the contribution due to the noise mean (if it is known a priori), or by introducing a DC block in the frequency plane of the correlator. This second approach is *robust* to uncertainties in the first order characteristics of the noise.

2.4. Efficient Algorithm for OPOFs

2.4.1. Algorithm

In this section, we provide an efficient numerical procedure for finding the support of the OPOF when the noise is white. Then, the denominator in Eq. (2.11) depends *only* on the *area* of the support and *not* on which exact spatial frequencies are included in this support. Thus, for a given size of the support, we want to include those spatial frequencies that maximize the numerator of Eq. (2.11). To do this on a digital computer, we use the discrete notation. To accomplish this, we reorder the samples of the signal Fourier transform as below.

$$| S(1) | \geq | S(2) | \geq \cdots \geq | S(d) | \quad , \tag{2.64}$$

where d is the number of samples in the signal discrete Fourier transform (DFT) $S(k)$. Let K denote the number of pixels in the support. By choosing the K pixels corresponding to the first K signal DFT values in Eq. (2.64), we will maximize the resulting SNR for that choice of K. The corresponding SNR is given by

$$\mathrm{SNR}\,(K) = \frac{\Delta f}{N_0 K} \left[\sum_{k=1}^{K} | S(k) | \right]^2 \quad , \tag{2.65}$$

where Δf is the integration step size, and can be ignored in the optimization procedure. We numerically evaluate $\mathrm{SNR}\,(K)$ for all possible choices of K and select the one that

maximizes it. Notice that without the ordering scheme, for each value of K we must try all possible supports consisting of K pixels. This is impossible even for small K values.

2.4.2. Simulation Results

In this section, we investigate the comparative performance of the classical matched filter (MSF), the conventional phase-only filter (POF) and the optimal phase-only filter (OPOF) with the help of realistic 2-D images.

2.4.2.1. Tank Image

In this simulation example, we used the 32×32 tank image shown in Figure 2-3. All

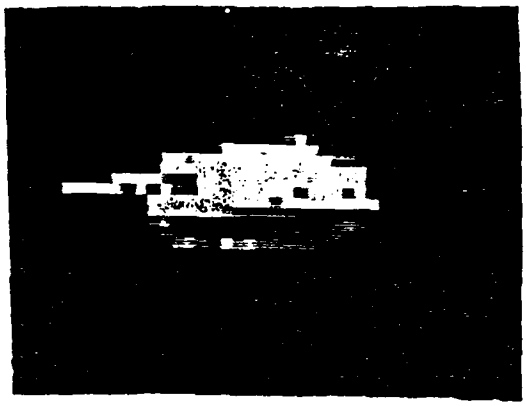

Figure 2-3: Tank image used.

three types of correlations (the MSF, the POF and the OPOF) were done with the help of FFTs of size 64×64. The original 32×32 images (both the reference images and the observed images) were converted to 64×64 images by padding them with zeros. To investigate the effects of various amounts of noise, we added zero-mean, Gaussian, white noise of variance σ^2 to these images. Sample images obtained by adding noise realizations of variances 1, 2, 5, 10, 50, 100, 200, 500 and 1000 are shown in Figs. 2-4(a) through 2-4(i), respectively. It was seen that the uncorrupted image in Fig. 2-3 has an average pixel energy of 119.7; thus, a noise variance of 100 represents an input SNR of 10 $\log_{10}$ $(119.7/100) = 0.781$ dB.

The magnitude of the 2-D Fourier transform of the image in Fig. 2-3 is shown in Fig.

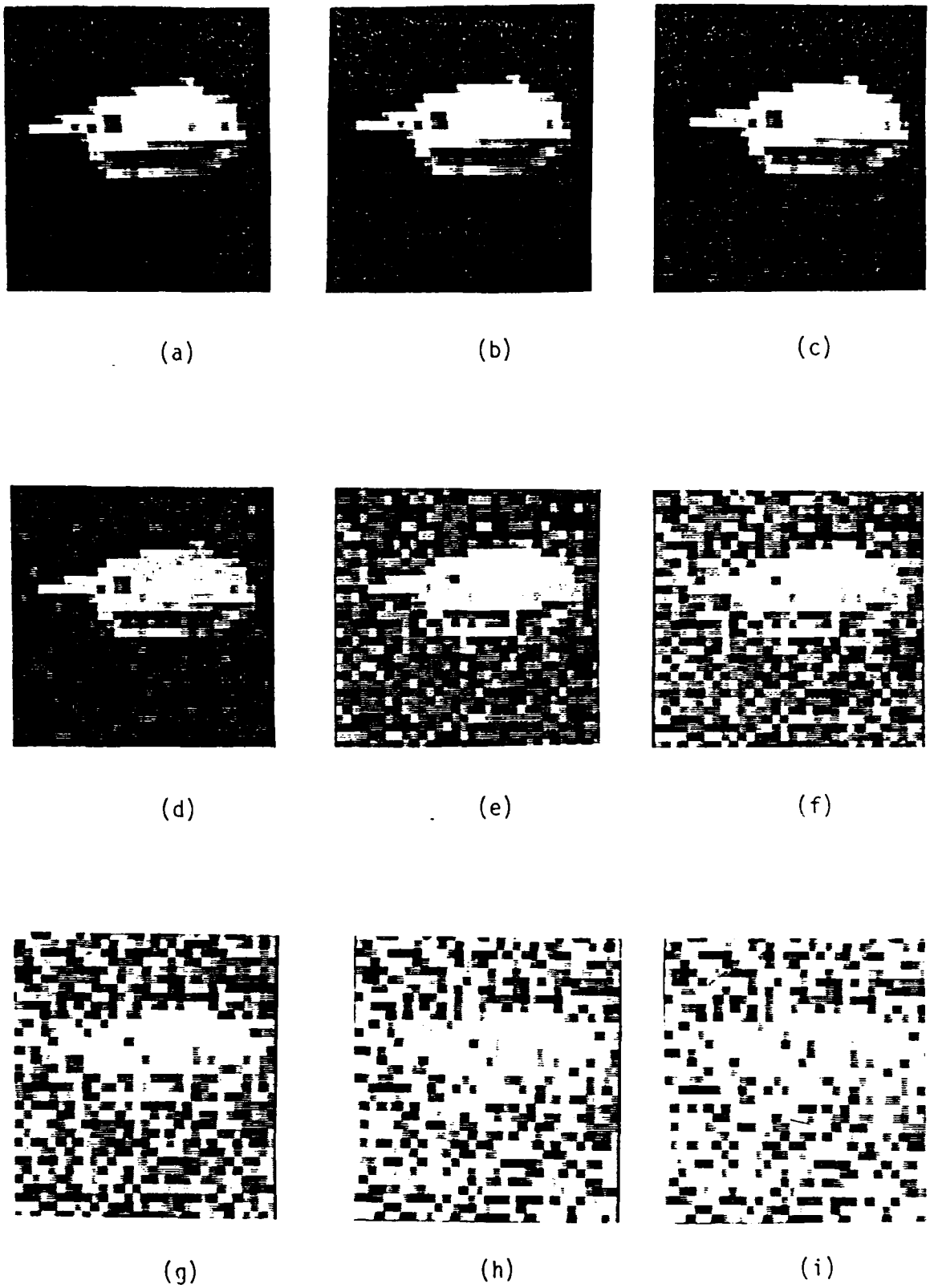

Figure 2-4: Noisy tank images.

Figure 2-5: Magnitude of the FT of tank image.

2-5. Because of the limited dynamic range of the display device, we do not see the high dynamic range of this FT magnitude (maximum value of 4040, minimum value close to zero) in this figure. This high dynamic range is a direct consequence of the nonzero average value in the original image We avoided the deliberate introduction of low-frequency stops in the filter plane (usually done in optical matched filtering) since it interferes with the OPOF optimality by introducing an ad-hoc intermediate step. The phase of the resulting POF is shown in Fig. 2-6 where darker regions represent phases close

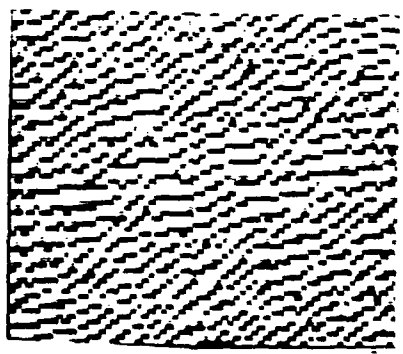

Figure 2-6: Phase of POF for tank image.

to $-\pi$ and brighter regions represent phases close to $+\pi$. The OPOF has the same phase characteristic as the one shown in Fig. 2-6 except that its magnitude is nonzero only over a smaller frequency region. We numerically determined the support of this OPOF to

maximize the output SNR. The resulting support is shown in Fig. 2-7. It is not surprising to see that the OPOF allows only those regions where the image FT magnitude is very large.

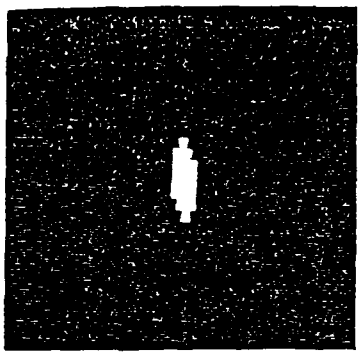

Figure 2-7: Optimal support for tank image.

The SNRs obtained with the three different filters were evaluated by repeating the above cross-correlation experiments with 100 different noise realizations. The average value of the output correlation at the origin as well as its variance were used in estimating the SNR. The output SNR as a function of the input SNR (over the range of -10 dB to +20 dB) is shown in Fig. 2-8 for the three different filters. The SNR relation given in Eq. (2.47) is illustrated very clearly in Fig. 2-8. We see from this figure that the matched filter yields a processing gain (output SNR in dB minus input SNR in dB) of about 30 dB, which is the expected SNR improvement for an image with about 1024 pixels. The conventional POF yields a processing gain (PG) of 25 dB whereas the optimal POF yields a PG of about 28.5 dB. Thus, use of the OPOF improves the SNR by about 3.5 dB compared to that obtained by the conventional POF. This improvement is quite significant.

It is easily seen that the OPOF has a smaller bandwidth compared to the conventional POF. Thus, we can expect that the correlation peaks obtained from the OPOF to be broader. To illustrate this, we include sample cross-correlations obtained from the three methods in Figs. 2-9 and 2-10. Figs. 2-9(a), 2-9(b), and 2-9(c) show the three output correlations when the input noise is of variance 100 (input SNR is 0.78 dB).

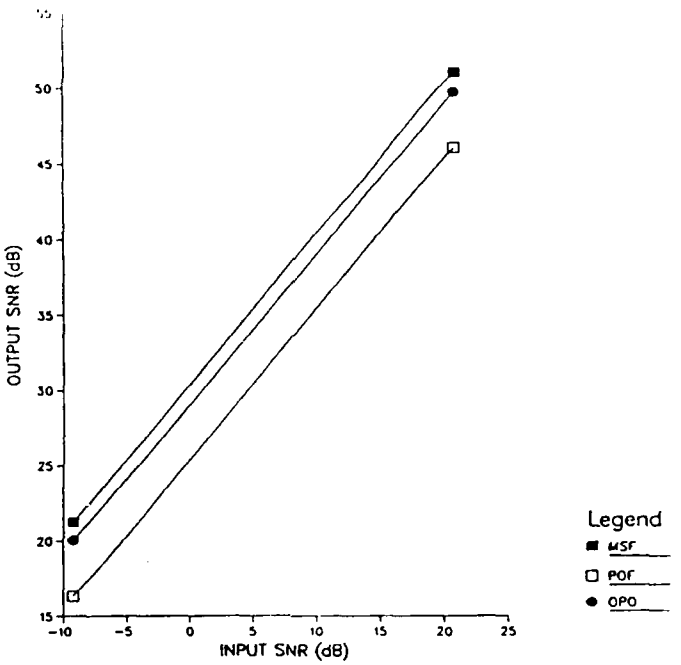

Figure 2-8: Output SNR (vs) input SNR for tank image.

Similarly, Figs. 2-10(a), 2-10(b), and 2-10(c) show the output correlations when the input noise is of variance 1000 (input SNR is -9.22 dB). We see from Fig. 2-9 that the conventional POF yields the sharpest correlation peak whereas the OPOF yields broad correlation peaks. The sidelobe structure is seen to be the most oscillatory for the conventional POF and less oscillatory for both the OPOF and the classical matched filter. This behavior is much more pronounced in Fig. 2-10 where the input noise has a variance ten times as high as the one in Fig. 2-9.

2.4.2.2. Pliers Image

In this second simulation example, we used the 32×32 pliers image shown in Fig. 2-11. This image had average pixel energy of 120.68. We carried out the same simulation steps described above (i.e., same FFT size, noise variances, number of realizations...,etc.). Fig. 2-12 shows the magnitude of the Fourier transform of the image in Fig. 2-11. As can be observed, the vertically elongated pliers image yields a horizontally elongated Fourier transform. The negative of the phase of the Fourier transform is shown in Fig. 2-13 The

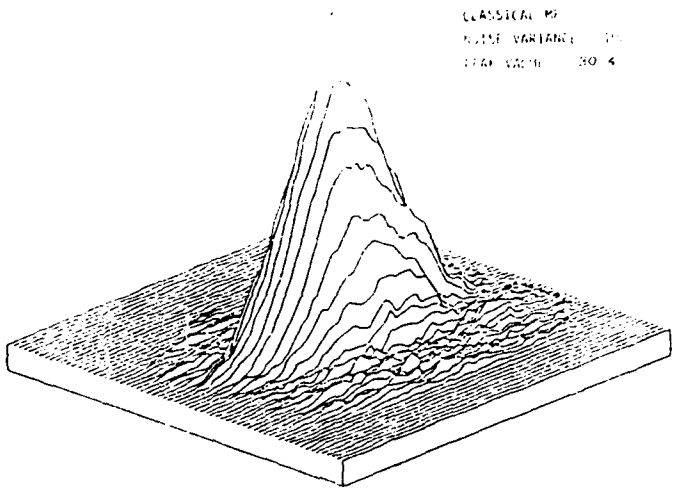

(a)

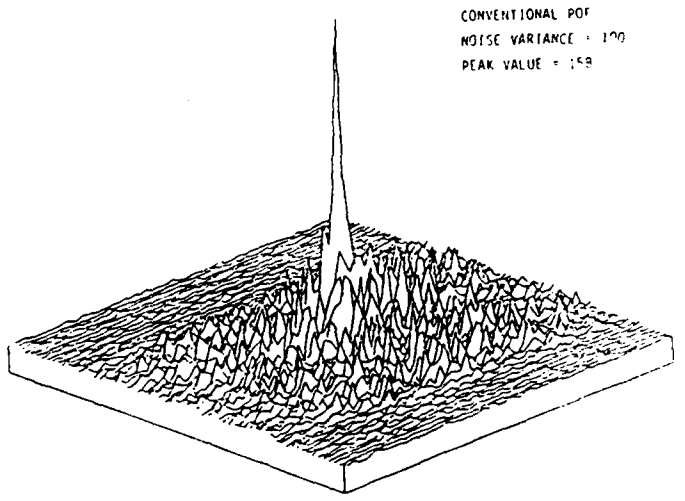

(b)

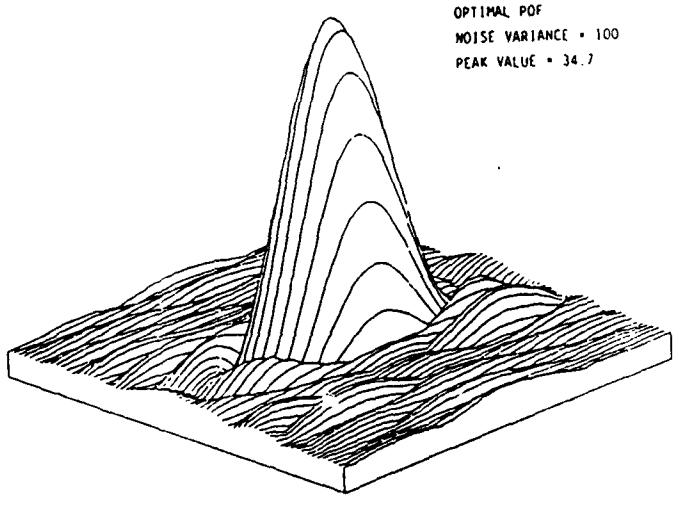

(c)

Figure 2-9: Output correlation of tank image with MSF, POF, and OPOF when input noise is of variance 100.

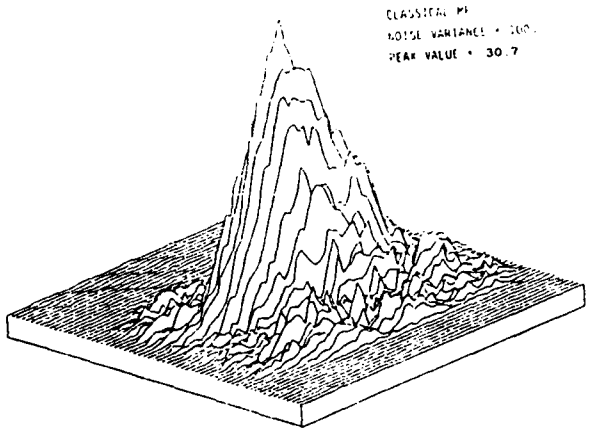

(a)

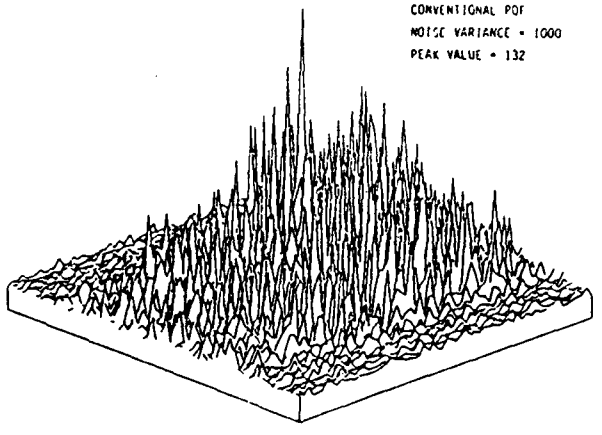

(b)

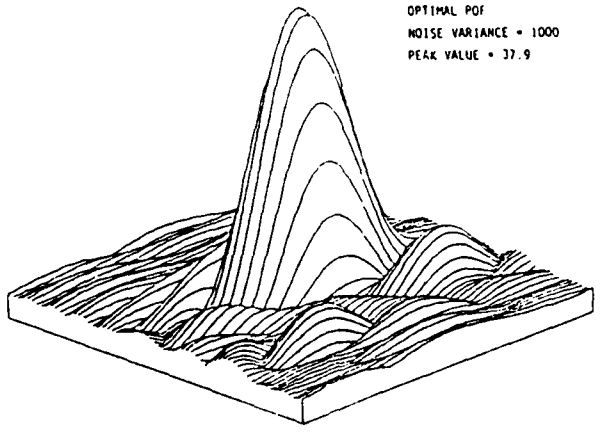

(c)

Figure 2-10: Output correlation of tank image with MSF, POF, and OPOF when input noise is of variance 1000.

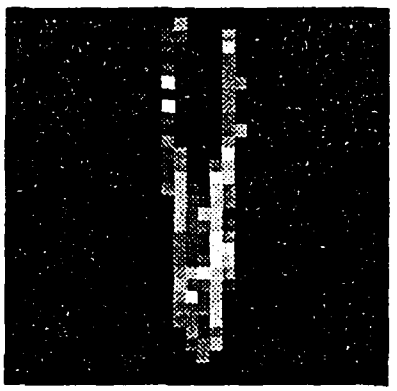

Figure 2-11: Pliers image used.

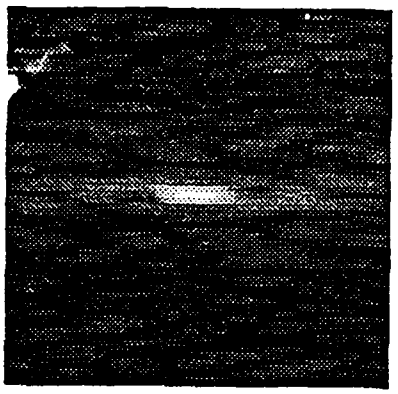

Figure 2-12: Magnitude of the FT of pliers image.

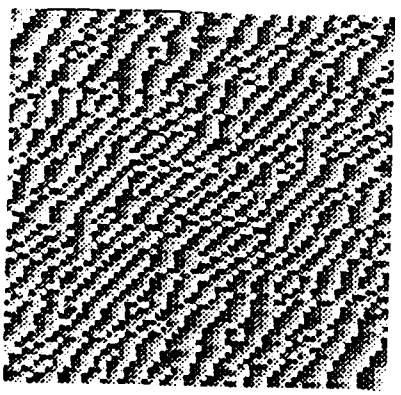

Figure 2-13: Phase of POF for pliers image.

numerically found optimal support for the pliers image is shown in Fig. 2-14. It consists of 311 pixels that are "ON". It is intersting to observe that the support for this case is a

multi-pass region. This is contrary to the intuitive idea of using a low pass filter for noise reduction in images. Nevertheless, it is seen that the support is still emphasizing those regions in frequency (including DC) where most of the energy in the image lies. This is a direct consequence of the fact that we are optimizing the signal-to-noise ratio, since the SNR increases with the amount of signal energy reaching the output. However, as we will see shortly, in a classification problem the frequencies that carry most of the energy in the filter may not coincide with the frequencies that carry most of the *discriminatory information*. Hence, we expect in such cases that the optimal support will exhibit an even more "scattered" behavior.

Figure 2-14: Optimal support for pliers image.

We computed estimates of output SNRs with all three filters (MSF, POF, and OPOF) as we did in the previous simulation example. These output SNRs are plotted as a function of input SNRs in Fig. 2-15. This figure shows the same hierarchy observed earlier in Fig. 2-8. The Matched filter yielded the highest SNR with a processing gain (PG) of about 30.5 db. Next, comes the OPOF with a PG 2 db below that of the matched filter. Finally, the POF comes last with a PG 1.5 db below that of the OPOF. Hence, optimizing the pass band resulted in improving the output SNR by about 1.5 dB. Even though this is less than the 3.5 dB improvement obtained earlier with the tank image, it is still considered significant.

The image examples used in the above simulations clearly illustrate the superiority of the OPOF over the conventional POF when the output SNR is the criterion of interest.

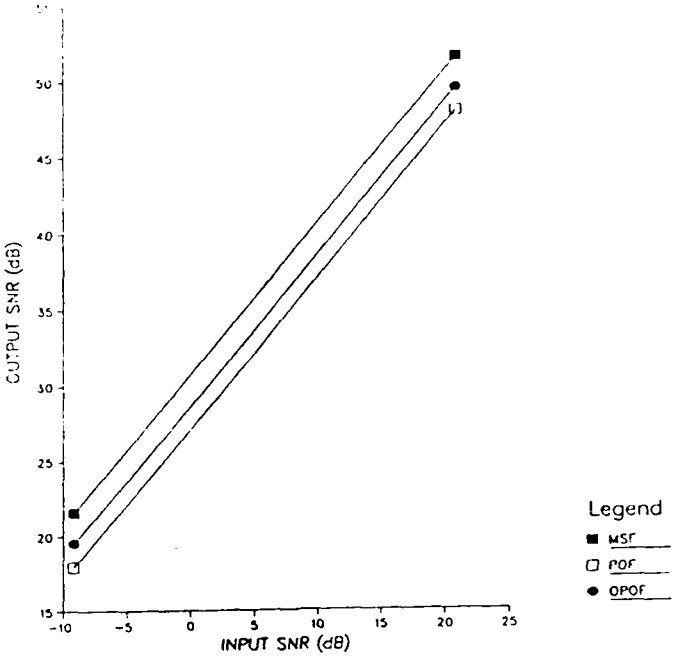

Figure 2-15: Output SNR (vs) input SNR for pliers image.

2.4.3. Window Approximation to Support

Realistic images have most of their energy lying in the low frequency region of the spectrum. This fact often allows filter designers to use low frequency (square) windows to reject the corruptive high frequency components. Hence, our support optimization might be initially taken to fall in the realm of the well known practice of using a low pass window to cut-off high frequency noise. However, the above simulation examples clearly illustrate that there is a definite structure in the solved for supports. This structure could not be predicted ahead of time, and leads to SNR values higher than those obtained using any other window function.

Nevertheless, the square type of windows is easier to implement in an optical correlator[ix] than the rather arbitrarily shaped supports shown above. Hence, there is a

[ix] This is particularly true for optical correlators based on the grid structured Spatial Light Modulators (SLMs) which will be introduced in the coming chapters.

trade-off between the ease of filter implementation and the resulting SNR. It seems therefore legitimate to ask: If one constrains the support to be square, how much SNR do we give up?

We addressed this problem numerically using the same two images. We assumed white noise in all cases. To find the best square window, we first start with a 3×3 window centered around the origin and numerically compute the resulting SNR using the discrete version of the SNR expression given in Eq. (2.2). Then, we enlarge the window to 5×5 and find the corresponding SNR. We keep enlarging the window (while ensuring that it remains centered around the origin) and each time we compute the corresponding SNR. The best square window is the one that leads to the highest SNR.

We first used the tank image shown in Fig. 2-3. The best square window was found to be of size 7×7, hence leading to 49 pixels that are "ON". The SNR corresponding to this window was numerically computed and found to be 1.5 dB below that resulting from the optimal support presented earlier (which had 59 pixels "ON"). This drop in SNR was verified by running the same simulations presented earlier, wherein the tank image is corrupted by the same type of noise with the same variance increments (1, 2, 5, 10, 50, 100, 200, 500, 1000). With each variance value, the output SNR with all four available filters, namely MSF, POF, OPOF, and POF_w (denoting the "window" filter) is estimated by averaging over 100 noise realizations. Figure 2-16 plots these output SNRs as a function of input SNRs. It confirms that SNR_{POF_w} is about 1.5 dB below SNR_{OPOF} which is about 1.3 dB below SNR_{MSF}. At the bottom of the hierarchy, comes the POF with an output SNR approximately 2.5 dB below that of POF_w.

This procedure was performed again on the pliers image. The best square window size was found to occupy the whole array (i.e., 64×64). Hence, POF_w is identically equal to POF in this case. Thus, imposing the square shape on the support incurred a drop of about 1.8 dB in SNR relative to the OPOF. The simulation results were already presented in Fig. 2-15.

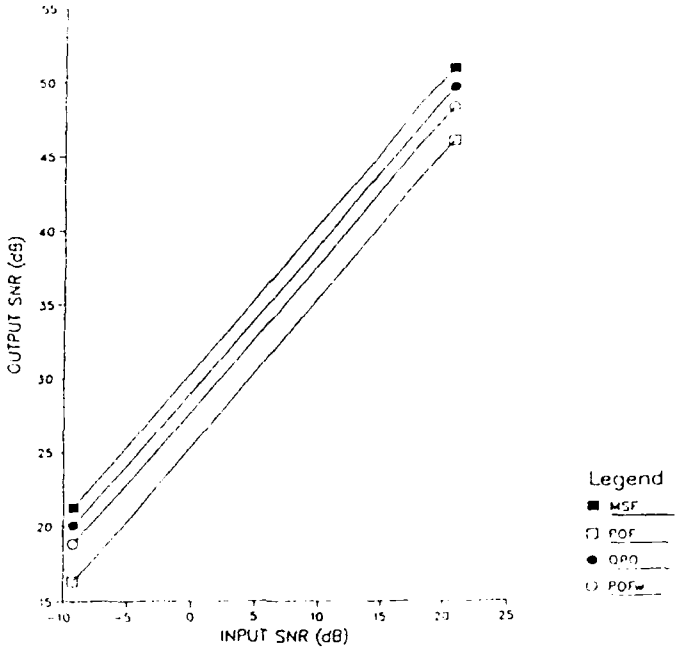

Figure 2-16: Output SNR (vs) input SNR for MSF, POF, OPOF, and POF_W using tank image.

The above discussion points out that the price of using (the easier to implement) square window can be as high as 1.8 dB loss in SNR. It is up to the designer to judge if this loss is worth the advantages acquired in practice. It is worthwhile also pointing out that this window approximation makes sense only when most of the energy in the filter lies at low frequencies. This however may not always be true. This is especially true for two class problems in which the frequencies of interest shift to the high frequency range since it is believed to contain most of the discriminatory information.

2.5. Very Efficient Sub-optimal Technique for OPOF Design

In this section, we develop a very efficient sub-optimal algorithm for support optimization in OPOFs. However, before presenting the new algorithm, a subtle point has to be addressed. The efficiency of the new algorithm will be measured with respect to the "old" one. Hence, if the latter is not as efficient as it can be, our evaluation of the new

algorithm will be biased. Therefore, the first thing to do is to "polish" the old algorithm and ensure that it is as close as possible to its most efficient form.

2.5.1. Enhancing the Old Algorithm

Examination of that algorithm (Section 2.3) reveals that the most time consuming part is the sorting procedure. We have been using the *Selection Sort*[21] procedure, which, like the *Quick Sort*, *Merge Sort*, *Shell Sort*, and *Bubble Sort* has a worst case number of iterations of the order of N^2, where N is the number of entries being sorted. A brief literature search showed that the most efficient sorting algorithm known so far is the *Heap Sort*[22]. This algorithm has a *worst case* number of iterations of the order of $N\,log_2(N)$. Essentially, the numbers to be sorted are not regarded as an array, but as a binary tree. The idea is to give this tree a specific structure (called a *Heap*) wherein every "father" node is greater than or equal to its "son" nodes. It turns out that to place each number in its right position, one only needs to perform a number of comparisons that is, in the worst case, proportional to the number of "levels" (equal to $log_2(N)$) in the heap. This is where the efficiency of this algorithm comes from.

We used the heap sort in our old algorithm and noticed a substantial reduction in the computing time. For example, to compute the optimal support for the 32×32 image shown earlier (Fig. 2-3) on which a 64×64 FFT was performed, it used to take around 293 seconds on a VAX 11/750. Using the heap sort, this number was reduced to just over 10 sec. When using a 128×128 FFT size, computing the optimal support used to take about 11630 seconds. With the heap sort, this number was reduced to only 65 seconds. Even though we cannot claim our old algorithm is now as efficient as it can get since other fine enhancements can still be applied , we feel it is very close to its most efficient form. Hence, we now think it is fair to measure the performance of the algorithm we are about to introduce to our improved old algorithm.

2.5.2. Analysis

Let us recall that in support optimization, our objective is to find K_{opt} that optimizes the SNR given by

$$SNR(K) = \frac{\left[\sum_{i=1}^{K} |S(i)|\right]^2}{K} , \tag{2.66}$$

where in Eq. (2.66) we assume the numbers $|S(i)|$ ($i = 1, ..., d$) have been sorted in descending order. The following proposition provides some insight about the optimal support and should help in the above optimization.

Proposition 3: If two or more pixels have equal magnitudes, either *all* or *none* of them are included in the optimal support.

Proof: It is sufficient to prove the above result for two pixels only. The case of three or more pixels easily follows by *deduction*. Assume $|S(K_o)| = |S(K_o+1)|$ for some $K_o \geq 2$ ($K_o = 1$ is a trivial case proved easily). There are two cases. The first, is that

$$SNR(K_o) \geq SNR(K_o-1) . \tag{2.67}$$

We now propose to show that in this case $SNR(K_o+1) \geq SNR(K_o)$, hence implying to include both K_o and K_o+1 in the optimal support. Let

$$\beta = \sum_{i=1}^{K_o} |S(i)| . \tag{2.68}$$

Using Eq. (2.68) in Eq. (2.66), we get

$$SNR(K_o+1) - SNR(K_o)$$

$$= \frac{(\beta + |S(K_o)|)^2}{K_o + 1} - \frac{\beta^2}{K_o}$$

$$= \frac{1}{K_o(K_o+1)} [K_o(\beta^2 + |S(K_o)|^2 + 2\beta|S(K_o)|) - (K_o + 1)\beta^2]$$

$$= \frac{1}{K_o(K_o+1)} [K_o(|S(K_o)|^2 + 2\beta|S(K_o)|) - \beta^2] \ . \qquad (2.69)$$

Using (2.66), (2.67), and (2.68), we obtain

$$SNR(K_o) - SNR(K_o-1) \ \geq \ 0$$

$$\Leftrightarrow \frac{\beta^2}{K_o} - \frac{(\beta - |S(K_o)|)^2}{(K_o-1)} \ \geq \ 0$$

$$\Leftrightarrow \frac{1}{K_o(K_o-1)} [(K_o-1)\beta^2 - K_o(\beta^2 + |S(K_o)|^2 - 2\beta|S(K_o)|)] \ \geq \ 0$$

$$\Leftrightarrow -\beta^2 + K_o(2\beta|S(K_o)| - |S(K_o)|^2) \ \geq \ 0$$

$$\Rightarrow K_o(2\beta|S(K_o)| + |S(K_o)|^2) - \beta^2 \ \geq \ 0 \ . \qquad (2.70)$$

Eqs. (2.69) and (2.70) together imply the sought after result.

Now, the second case is that

$$SNR(K_o) \ < \ SNR(K_o-1) \ . \qquad (2.71)$$

In this case, it is not difficult to see[vi] that

$$K_{opt} \ < \ K_o \quad \text{or} \quad K_{opt} \ \geq \ K_o + 1 \ , \qquad (2.72)$$

indicating that either both pixels K_o and $K_o + 1$ or none of the two are included in the optimal support •

[vi] Note that for a "cluster" of three or more pixels having the same magnitude, K_{opt} cannot be in the "interior" of this cluster by the argument given in case 1.

The above proposition suggests an interesting idea. Suppose we quantize $|S(i)|$, $i = 1,..., d$ into N levels. Then, we do not have to compute the SNR for all d pixels. It is enough to compute the SNR for the N quantization levels only, knowing from the above proposition that pixels with the same quantization level will either all or none be included in the optimal support. Hence, we are ready to present a new, *very efficient* sub-optimal algorithm for POF support selection. The efficiency of this new algorithm stems from the fact that it is, in principle, independent of the number of pixels and depends primarily on the number of quantization levels which is expected to be smaller than the number of pixels ($>$4000) for practical cases. The sub-optimality of this new algorithm is due to the approximation that all pixel magnitudes falling in the same quantization level are equal. This approximation can be made more accurate by increasing N (the number of quantizations).

2.5.3. Algorithm

Below, we list the steps of our new algorithm.

- STEP 1: /* This normalizes and initializes variables*/

  Normalize $|S(\,I\,)|$, I=1,...,d.
  LEVEL(I)=0, I=1,...,(N-1).
  TAG(I)=0, I=1,...,d.
  COUNT=0; SUM=0; SNR=0; I=0.

- STEP 2: /*This assigns levels to pixels*/

  I=I+1
  J=$|S(\,I\,)|$ * (N−1).
  IF J $\neq$ 0, LEVEL(J)=LEVEL(J)+1.
  TAG(I)=J
  IF I<d, GO TO STEP 2.
  I=N-1

- STEP 3: /* This gets the optimal level*/

  I=I-1
  COUNT=COUNT+LEVEL(I)

SUM=SUM+LEVEL(I)*I
TEMP=$(SUM)^2$/COUNT
IF TEMP>SNR, INDEX=I; SNR=TEMP.
IF I>1 GO TO STEP 3.
I=0.

- STEP 4: /* This gets the optimal support*/

I=I+1
IF TAG(I) $\geq$ INDEX, INCLUDE I IN SUPPORT.
IF I<d, GO TO STEP 4

- STEP 5: END.

2.5.4. Numerical Results

We have implemented and tested this new algorithm. The results are impressive. For example, using the same tank image with an FFT of size 64×64 and using N=256 levels, we obtained in 0.13 seconds the same support we got previously in 10.15 seconds with the old (improved) algorithm. This is a reduction in CPU time by a factor of 78. As already mentioned, we expect this factor to increase even further as the number of pixels increase. To test this, we increased the size of the FFT to 128×128 and applied our new algorithm with N=256. It took 0.5 seconds to find a support made of 235 pixels to yield a numerically computed SNR (assuming unit variance white noise) of 76.46116 (=18.834409 dB). Using the improved old algorithm, it took 64.6 seconds to find the optimal support consisting of 237 pixels to yield a numerically computed SNR of 76.46427 (=18.834585 dB). The new algorithm has now achieved a time reduction factor of almost 130! There is a small price though. We have given up about 0.00018 dB in SNR. In case this loss does not seem negligeable enough, one can slightly increase N to reduce the inaccuracy in the new algorithm. For example, by increasing N from 256 to 400, we obtained the optimal support exactly (i.e., 237 pixels) in practically the same CPU time (0.5 second).

A comment is due at this point. It seems that as the number of pixels further increases, this reduction factor increases even further. We increased the FFT size to

256×256. The old algorithm took 304.33 seconds to generate the optimal support (931 pixels) to yield a numerically computed optimal SNR of 76.422375 (=18.832205 dB). Applying the new algorithm with N=256, it took 2.88 seconds to find a support made up of 921 pixels to yield an SNR of 76.419975 (=18.832069 dB). This results in a reduction factor of about 106 with a loss in SNR of about 0.00014. Increasing N to 1000 achieved an exact solution in 2.93 seconds (a time reduction of about 104). Thus, the time reduction factor has dropped from 130 to 104 as we quadrupled the number of pixels. We believe this behavior is due to the overhead computations (such as assignments) that seems to "take over" as the number of pixels increase, hence causing the time reduction factor to exhibit a "peak". Notice also how the number of quantization levels necessary to achieve exact results slowly increases with the number of pixels, while the computation time difference increases very slowly. This may suggest an enhancement to the new algorithm by *adaptively* changing N (eg. N= a slow function of d).

Before moving to the next section, a last assessement of the new algorithm is due. It seems that this newly proposed algorithm has provided us with tremendous savings in computer time (about two orders of magnitude) at the expense of a very small loss in SNR (less than 2×10^{-4} dB). As argued above, we can even get exact results with a saving of at least one order of magnitude in computer time (this being a rather conservative number). What did we give up? The answer is *nothing*. The only other point that could be a price is the memory requirement of the algorithm. It turns out that both the new and old algorithms use the same memory storage, since the d dimensional array that is used in the old algorithm for the sorting procedure is used in the new algorithm for tagging the pixels (i.e., to which level each pixel belongs). It is worthwhile mentioning that all the CPU times presented above do not take into account the time to compute the FFT, get the magnitude of the pixels and normalize them, and the input/output operations. All these computations are common to both algorithms and strictly speaking do not constitute part of the algorithms themselves.

2.6. Distortion Sensitivity of OPOF

As mentioned earlier, one of the main problems associated with POFs is their sensitivity to input distortion. This problem seems to be related to the implicit high frequency emphasis described previously. In this section, we propose to investigate the distortion sensitivity of POFs relative to the OPOF and Matched filter using computer simulations. In the first run, we used a data base consisting of distorted versions of the tank image shown in Fig. 2-3. The distortion we deal with here is 3-D rotation. All images are pictures of the tank viewed along a "cone" with 10° degree rotation increments. The tank is viewed with a depression angle of 70° with respect to ground. We computed estimates of output SNRs for the first 12 images (corresponding to rotation angles of 0° to 110°) as follows. First, we corrupt each image with independent zero-mean noise having a variance of 50 (this corresponds to an average input SNR of about 3 dB). Next, the corrupted image is zero padded and a 64×64 FFT is performed. This is used to obtain the correlation of the noisy input with all three filters (MSF, POF, and OPOF), and the value at the origin is registered. We repeat this process 100 times and find the average value of the output at the origin along with its variance. The ratio of the first quantity squared to the second gives an estimate of the SNR. Figure 2-17 shows the output SNRs of the three filters as a function of rotation in degree. It can be observed that the POF is the most sensitive filter to distortion in output SNR. The MSF and OPOF, on the other hand, exhibit a more tolerant behavior than POF. It is worthwhile to point out that the MSF in this case showed more tolerance to input rotation than has been previously reported[23]. The extreme sensitivity reported about MSFs[23] was for the case where the filter is optically recorded on a holographic plate, hence amplitude modulated on a high frequency carrier. The presence of this carrier causes the slightest mismatch between the input and the reference signals to considerably affect their correlations. This is not the case in our simulations wherein the MSF is simply stored as a complex array.

We further tested the relative sensitivity of POF with respect to MSF and OPOF on

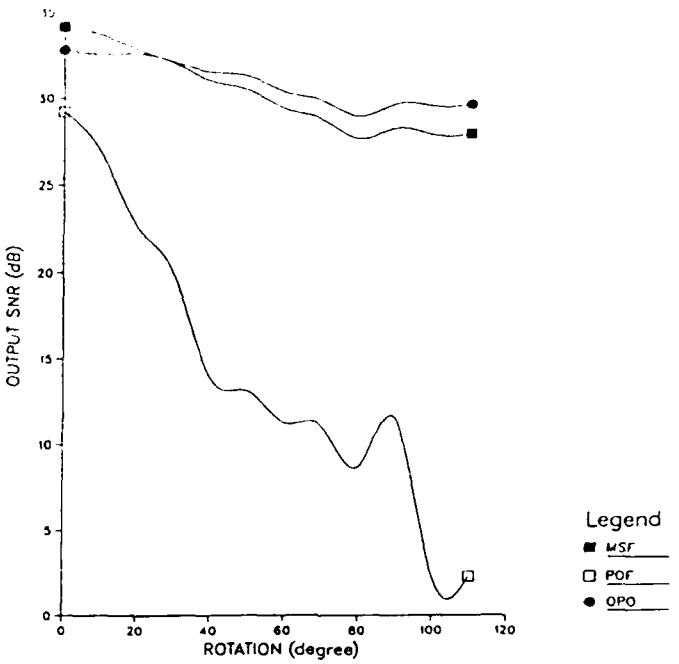

Figure 2-17: SNR (vs) input rotation for tank image for MSF, POF, and OPOF.

the pliers image. This time, the distortion consists of in-plane rotated versions of the image. We performed exactly the same simulation steps as described above. Fig. 2-18 summarizes our results. It essentially confirms the same conclusions drawn above about the sensitivity of POF. Note that in this case the OPOF and MSF exhibit more sensitivity than in the previous case. Nevertheless, their output SNR did not degrade as sharply as that of the POF. This is especially noticeable for input rotations between 0 and 30 degrees.

2.7. Two-class Problem

In a two-class discrimination problem (also referred to as generalized detection problem[4]), we have two hypotheses

$$H_1 : r(x) = s_1(x) + n(x) ,$$

and

$$H_2 : r(x) = s_2(x) + n(x) , \tag{2.73}$$

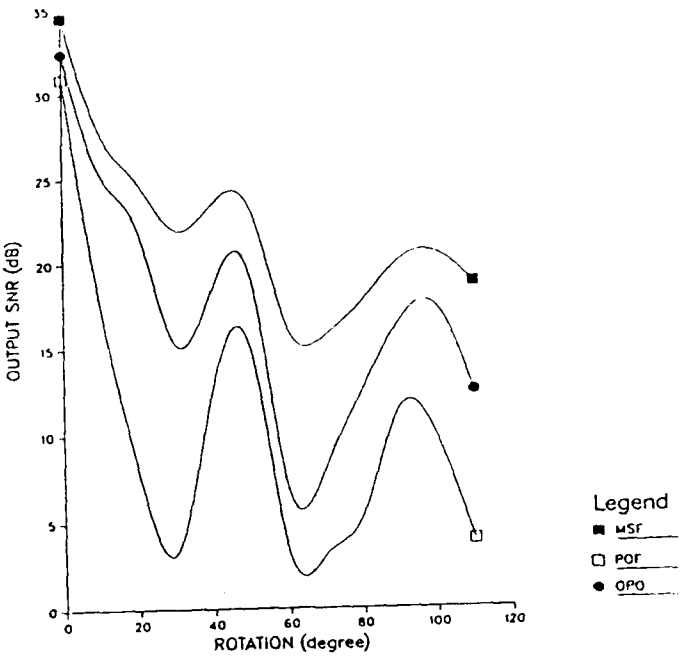

Figure 2-18: SNR (vs) input rotation for pliers image for MSF, POF, and OPOF.

where, $r(x)$ denotes the observed (or received) signal, $s_1(x)$ and $s_2(x)$ denote the two reference signal we deal with, and $n(x)$ a realization from a zero-mean random process with power spectral density $P_n(f)$. The objective is to use the observation $r(x)$ and, optimally, decide on which signal is present at the input, i.e., optimally discriminate between $s_1(x)$ and $s_2(x)$. For this purpose, we choose the filter transfer function $H(f)$ to maximize the SNR, now defined in its general context as

$$SNR = \frac{|E\{y(0)/\,\mathrm{H}_1\} - E\{y(0)/\,\mathrm{H}_2\}|^2}{var\{y(0)/\,\mathrm{H}_1\}} \,. \tag{2.74}$$

Eq. (2.74) can be written as

$$SNR = \frac{|\int_{\mathcal{R}} S_1(f)H(f)\,df - \int_{\mathcal{R}} S_2(f)H(f)\,df|^2}{\int_{\mathcal{R}} P_n(f)|H(f)|^2\,df}$$

$$= \frac{|\int_{\mathcal{R}} S'(f)\,H(f)\,df|^2}{\int_{\mathcal{R}} P_n(f)|H(f)|^2\,df}\,, \tag{2.75}$$

where,

$$S'(f) = S_1(f) - S_2(f)\,. \tag{2.76}$$

It can be seen from Eq. (2.75) that the SNR expression in this generalized context is identical to the SNR expression given in Eq. (2.2), except that the reference signal $s(x)$ in Eq. (2.2) is now replaced by the difference of the reference signals $s'(x) = s_1(x) - s_2(x)$. Hence, we expect all our earlier results to hold by using $s'(x)$ as our "reference" signal. Thus,

$$H_{opt}(f) = \alpha \frac{S'^*(f)}{P_n(f)} = \alpha \frac{(S_1^*(f) - S_2^*(f))}{P_n(f)}\,. \tag{2.77}$$

Likewise, the OPOF is given by (as in Eq. (2.7))

$$H_{\text{OPOF}}(f) = I_{\mathcal{R}_{opt}}(f)\; e^{-j\Phi_{s'}}\,, \tag{2.78}$$

where $\Phi_{s'}$ is the phase of $S_1(f) - S_2(f)$ and $\mathcal{R}_{opt}$ is the optimal support of the OPOF. Hence, all the techniques of OPOF design presented earlier can be applied in this context by using $s'(x) = s_1(x) - s_2(x)$ for our reference signal. In the following section, we present some computer simulations dealing with a 2-class problem.

2.7.1. Computer Simulations

We provide here the results of the computer simulations that were aimed at discriminating between the tank image shown in Fig. 2-3 and the Armored Personnel Carrier (APC) image shown in Fig. 2-19. Both images are 32×32 gray level with pixels ranging in intensity from 0 to about 60. To construct the matched filter and POF, we

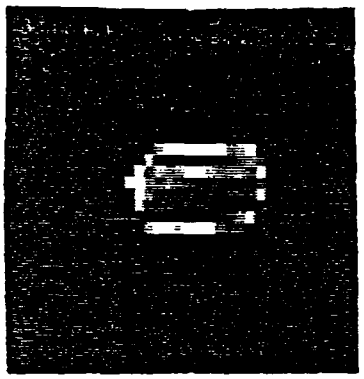

Figure 2-19: APC image used in the simulations.

generated a third "image" by subtracting the APC image from the tank. This image was then zero padded and a 64×64 FFT was performed. Fig. 2-20 shows the magnitude of the resulting Fourier transform. It can be seen that it is more "scattered" than the magnitude

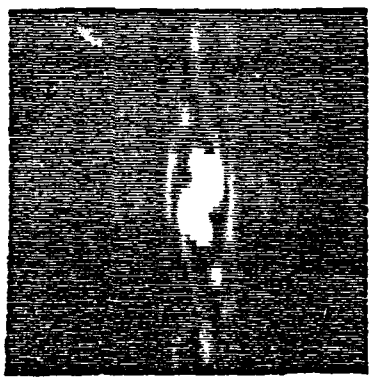

Figure 2-20: Magnitude of FT for difference between tank and APC.

of the FT for the tank image alone (shown in Fig. 2-5). The DC term has now dropped from about 4044 to about 1826. The dominance of the low frequency components has now decreased. This result agrees with the intuitive idea that discriminatory information lies

mostly at high frequencies (i.e., along the edges of the images)[xi]. Fig. 2-21 shows the phase of the POF (and OPOF), and Fig. 2-22 shows the optimal support generated by our algorithm. It has 1073 pixels "ON". It is interesting to observe that the optimal support now has a clear multiband structure, and that it is no longer emphasizing only low frequency components.

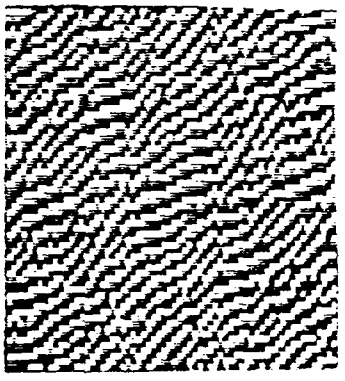

Figure 2-21: Phase of POF for tank (vs) APC.

Figure 2-22: Optimal support for tank (vs) APC.

To obtain estimates of output SNRs, we corrupt both the tank and APC with independent noise (with variance 1, 2, 5, 10, 50, 100, 200, 500, and 1000). The corrupted images are then zero padded to 64 by 64 and the output correlation (at the origin) of both the tank and APC with all three filters (MSF, POF, and OPOF) is *individually* recorded. We repeat this step 100 times for each variance. The output SNR corresponding to each

[xi] This can also be explained by the fact that since both tank and APC images are low frequency signals, taking their difference will cause the common components (namely DC and low frequency) to somewhat cancel out.

input noise variance is obtained by averaging the output associated with the tank and the APC, *taking their difference* squared and dividing it by the variance of either output (both variances should be equal). Fig. 2-23 summarizes our results. It can be seen, once again, that the MSF yields the highest SNR (with a PG of about 30.2 dB). Next comes the OPOF with 2 dB less SNR (with a PG of about 28.3 dB). Finally, the POF is 1 dB below the OPOF (the PG is about 27.3 dB). Thus, support optimization has provided us with a gain in SNR of 1 dB (versus 1.5 for the pliers and 3.5 dB for the tank).

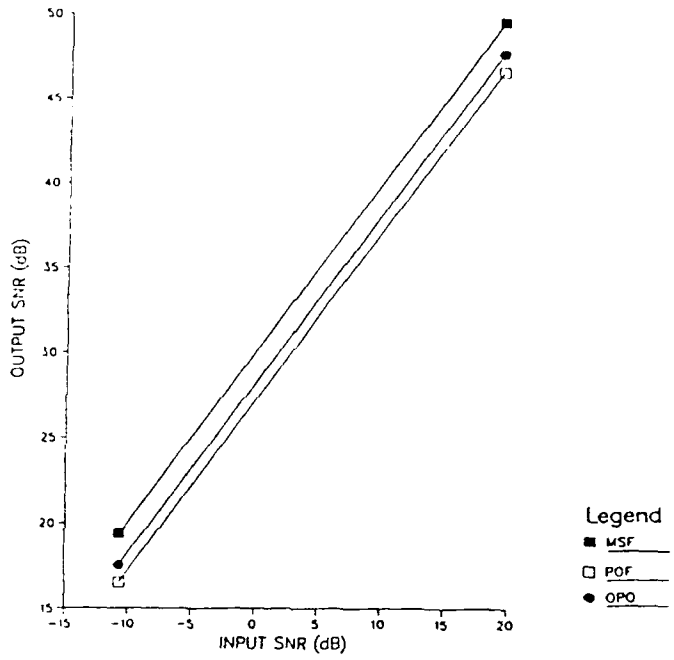

Figure 2-23: Output SNR (vs) input SNR for tank-APC.

2.8. OPOF With Detector Noise

2.8.1. Problem Formulation

As can be seen from Fig. 2-7, the OPOF has a much smaller support than the POF, and this will undoubtedly cause a decrease in light throughput. As a matter of fact, for this particular simulation example, the Horner[24] efficiency[viii] for the OPOF and POF was computed and found to be 70% and 100% respectively. If the goal in proposing phase-only filters is to seek higher light efficiency, amongst others, why reduce the filter's support as was done in OPOFs? Actually, when we derived the OPOF, our only criterion was the SNR in the correlation plane (prior to detectors) since we implicitly assumed that our output detectors are ideal. However, a more reasonable approach to this problem is as follows: Assume that the input image is corrupted by some additive noise, and that the output detector adds some noise (assumed to be independent of the input). Then we must determine the OPOF to minimize the probability of error.

Since we are considering only the detection problem, we will focus on the origin of the output correlation plane. We model the detector placed at the origin as providing a gain of α to the magnitude of the light falling on it and introducing detector noise n_{det}. For example, if light with magnitude A and phase θ (i.e., $A\,e^{j\theta}$) falls on the detector, then its output is given by

$$v_{det} = \alpha A + n_{det} . \tag{2.79}$$

where n_{det} is a zero-mean random variable with variance σ^2_{det} and is assumed to be independent of the light falling on the detector[ix].

[viii] The Horner Efficiency is defined as the ratio of the energy reaching the output plane to the energy in the input signal.

[ix] Actually, we expect the noise generated in the detector to depend on the strength of the signal generated by the incoming light. In other words, we expect this noise to be signal dependent. Unfortunately, this type of noise is much harder to analyze, and we need to make this simplifying assumption to be able to perform some analytical investigation of the problem.

Now, the observed signal (at the input of the correlator) consists of just noise (under hypothesis H_0) or the reference signal plus noise (under hypothesis H_1), i.e.,

$$\begin{aligned} H_0 &: \text{ (signal absent)} \quad r(x) = n(x) \\ H_1 &: \text{ (signal present)} \quad r(x) = s(x) + n(x) \ , \end{aligned} \tag{2.80}$$

where, $n(x)$ is a realization from a stationary random process with positive mean m_n and Power Spectral Density (PSD) $P_n(f)$, and $s(x)$ is the reference signal, which also has a positive DC value. Even stronger, we are assuming that both $n(x)$ and $s(x)$ are non-negative. This is in agreement with the fact that in practice, 2-D signals (images) are non-negative. Let $y_s(0)$ and $y_n(0)$ denote the output (that is just reaching the detector at the origin of the correlator plane) due to $s(x)$ and $n(x)$ respectively[x]. Explicitly, we have

$$y_s(0) = \int_{-\infty}^{\infty} S(f)H(f)\,df \ , \tag{2.81}$$

and

$$y_n(0) = \int_{-\infty}^{\infty} n(x)h(-x)\,dx \ , \tag{2.82}$$

where $h(x)$ is the impulse response of the filter placed at the frequency plane of the correlator. Note that $y_n(0)$ is a random variable with mean

$$m_{y_n} = m_n H(0) = m_n \int_{-\infty}^{\infty} h(x)\,dx \ , \tag{2.83}$$

and variance

---

[x]In the following, we shall assume that $y_s(0)$ and $y_n(0)$ are positive. While the solution that will be presented shortly guarantees that $y_s(0)$ is positive, it does not always yield a positive $y_n(0)$. However, one can argue from the fact that $n(x)$ is positive and that the p.d.f. of the random variable $y_n(0)$ is sharply centered around its (positive) mean, that the probability of $y_n(0)$ being negative is negligeable.

$$\sigma^2_{y_n} = \int_{-\infty}^{\infty} P_n(f)|H(f)|^2\, df \ . \tag{2.84}$$

Hence, under hypothesis H_0, the light falling on the detector is given by $y_n(0)$, and its output becomes

$$v_{det} = \lambda\, |y_n(0)| + n_{det} \ = \ \lambda\, y_n(0) + n_{det} \ . \tag{2.85}$$

The above v_{det} is a random variable with mean

$$E\{v_{det}/\, H_0\} = \lambda\, m_{y_n} = \lambda\, m_n H(0) \ , \tag{2.86}$$

and variance

$$var\{v_{det}/\, H_0\} = \lambda^2 \sigma^2_{y_n} + \sigma^2_{det} \ . \tag{2.87}$$

On the other hand, under hypothesis H_1, the light falling on the detector is equal to $y_s(0) + y_n(0)$, and its output becomes

$$v_{det} = \lambda\, |y_s(0) + y_n(0)| + n_{det} \ = \ \lambda\, y_s(0) + \lambda\, y_n(0) + n_{det} \ . \tag{2.88}$$

In this case, v_{det} is a random variable with mean

$$E\{v_{det}/\, H_1\} = \lambda\, y_s(0) + \lambda\, m_n H(0) \ , \tag{2.89}$$

and variance equal to the variance under hypothesis H_0.

Now, the objective is to find $H(f)$ to maximize the generalized SNR expression earlier defined in Eq. (2.74) and given by

$$SNR = \frac{(\lambda\, y_s(0))^2}{\lambda^2 \sigma^2_{y_n} + \sigma^2_{det}} \ . \tag{2.90}$$

Using Eq. (2.81) and (2.84) in Eq. (2.90) we get

$$SNR = \frac{\left[\int_{-\infty}^{\infty} S(f)H(f)\,df\right]^2}{\mathcal{Q}^{-1} + \int_{-\infty}^{\infty} P_n(f)|H(f)|^2\,df}\,, \tag{2.91}$$

where, the term $\mathcal{Q}$ in the above denotes the *quality* of the detector and is defined as

$$\mathcal{Q} = \frac{\lambda^2}{\sigma_{det}^2}\,. \tag{2.92}$$

The larger $\mathcal{Q}$, the better the quality of the detector since it implies more efficient and/or less noisy photo-electronic conversion.

2.8.2. OPOF derivation

In this section, our objective is to design an optimal phase-only filter that maximizes the SNR given in Eq. (2.91). Thus, we now constrain the filter used in the optical correlator to be of the form given in Eq. (2.7), namely

$$H(f) = \mathrm{I}_{\mathcal{R}}(f)\,e^{j\Phi(f)}\,, \tag{2.93}$$

where $\Phi(f)$ is the sought after phase of the OPOF, and $\mathcal{R}$ is its support, yet to be determined. Using Eq. (2.93) in Eq. (2.91), we get

$$SNR = \frac{\left[\int_{\mathcal{R}} S(f)e^{j\Phi(f)}\,df\right]^2}{\mathcal{Q}^{-1} + \int_{\mathcal{R}} P_n(f)\,df}\,. \tag{2.94}$$

It can be easily shown that the optimal phase function is given by

$$\Phi_{opt}(f) = -\Phi_s(f)\,, \tag{2.95}$$

resulting in the SNR expression (function of $\mathcal{R}$)

$$SNR_{\text{OPOF}} = \frac{\left[\int_{\mathcal{R}} |S(f)|\, df\right]^2}{\mathcal{Q}^{-1} + \int_{\mathcal{R}} P_n(f)\, df}. \tag{2.96}$$

Eq. (2.96) conveys the whole point behind designing OPOFs with detector noise. Even though the optimal phase in this case is identical to that found when no detector noise was taken in considerations, the optimal support is directly affected by the quality of the detector. This can be observed by letting $\mathcal{Q}$ approach infinity (i.e., the detector approaching an ideal one). Then, the SNR expression approaches that already derived without noise detector (given in Eq. (2.11)). Hence, we expect that as $\mathcal{Q}$ approaches infinity, the optimal support tends to that derived previously. On the other hand, as $\mathcal{Q}$ becomes smaller, the integral in the denominator of Eq. (2.96) becomes more negligeable and the optimal support $\mathcal{R}$ becomes larger. In the limiting case where $\mathcal{Q}$ approaches zero, the optimal support must be as large as possible since the variations of the integral in the denominator are neglected, and by using the largest support we get the largest possible numerator (even though the SNR will still tend to zero for practical finite energy spectra). In other words, what Eq. (2.96) conveys is that in situations where the detector is "good" we can focus mostly on the effect of the noise at the input and solve for the optimal support to minimize its effect. However, in situations where the detector is "bad" we should enlarge the optimal support so that more light reaches the output (hence the signal obtained at the output of the detector is stronger) and the SNR increases.

It can be once again easily shown that the optimal support is even symmetric for real reference signals and, for the case of white noise, can be written as the set of those frequencies at which the magnitude of the signal spectrum is above some threshold ϵ_o. Furthermore, if we assume the OPOF to be a low pass filter, then EQ. (2.96) can be written as

$$SNR_{\mathrm{OPOF}}(W_h) = 2\,\frac{\left[\int_0^{W_h} |S(f)|\,df\right]^2}{(2\,\mathcal{Q})^{-1} + \int_0^{W_h} P_n(f)\,df}\,, \tag{2.97}$$

where W_h above refers to the cut-off frequency of the OPOF. To find the optimal W_h, we set the derivative of the SNR in Eq. (2.97) with respect to W_h to zero. Thus, W_h is the solution to the following transcendental equation.

$$\frac{2}{P_n(W_h)}\int_0^{W_h} P_n(f)\,df \;+\; (\mathcal{Q}\,P_n(W_h))^{-1} \;=$$

$$\frac{1}{|S(W_h)|}\int_0^{W_h} |S(f)|\,df\,. \tag{2.98}$$

Once again, it can be seen that as $\mathcal{Q}$ above approaches infinity (i.e., ideal detector), Eq. (2.98) becomes identical to Eq. (2.37).

2.8.3. Analytical Examples

We now consider some analytical examples to illustrate the design of OPOF support in the presence of detector noise.

2.8.3.1. Triangular Spectrum

We consider in this example the same triangular signal spectrum given in Eq. (2.41). We assume the input noise to be white with level N_0. Thus, Eq. (2.98) yields

$$\frac{2}{N_0} N_0 W_h + (\mathcal{Q} N_0)^{-1} = \frac{1}{1 - W_h/W_s} \int_0^{W_h} (1 - f/W_s)\, df$$

$$\Leftrightarrow \quad 2W_h(1 - W_h/W_s) + (\mathcal{Q} N_0)^{-1}(1 - W_h/W_s) = W_h - W_h^2/(2 W_s)$$

$$\Leftrightarrow \quad (3\, \mathcal{Q} N_0/2)\, W_h^2 - (\mathcal{Q} N_0 W_s - 1) W_h - W_s = 0$$

$$\Rightarrow \quad W_h = \frac{\mathcal{Q} N_0 W_s - 1 + \sqrt{(\mathcal{Q} N_0 W_s)^2 + 4 \mathcal{Q} N_0 W_s + 1}}{3 \mathcal{Q} N_0} . \tag{2.99}$$

Some interesting observations can be made from Eq. (2.99).

- Unlike previously, W_h now depends on all parameters, including N_0, the noise PSD level.
- For all non-zero values of $\mathcal{Q}$, N_0, we have

$$\frac{2}{3} W_s < W_h < W_s . \tag{2.100}$$

- As $\mathcal{Q} N_0$ approaches infinity (indicating the detector is approaching an ideal detector and/or the input noise power is getting larger), W_h approaches $2 W_s/3$. This is the cut-off previously derived with no detector noise considerations. Thus, large values of $\mathcal{Q} N_0$ call for more emphasis on the input noise.
- As $\mathcal{Q} N_0$ approaches zero (indicating the detector is approaching a very "bad" detector and/or the input noise power is getting smaller), W_h approaches W_s. This is the largest cut-off frequency that can be achieved. Thus, low values of $\mathcal{Q} N_0$ call for more emphasis on the detector noise by asking for a larger support than it would normally be without detector noise considerations.
- W_h *monotonically* decreases with $\mathcal{Q} N_0$.

The last three observations are summarized by the plot of W_h as a function of $\mathcal{Q} N_0$ shown in Fig. 2-24.

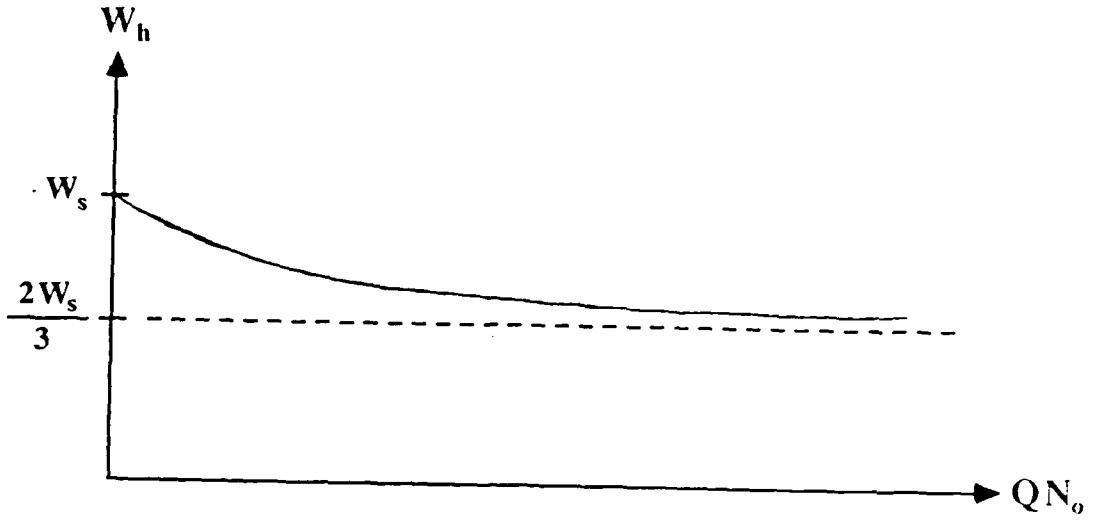

Figure 2-24: Plot of W_h as a function of $\mathcal{Q}N_0$.

2.8.3.2. Cosinusoidal Spectrum

In this example, we consider the cosinusoidal signal spectrum given in Eq. (2.48), with a white noise of level N_0. Eq. (2.98) yields

$$\frac{2}{N_0} N_0 W_h + (\mathcal{Q} N_0)^{-1} = \frac{1}{\cos(\pi W_h / 2W_s)} \int_0^{W_h} \cos(\pi f / 2W_s)\, df$$

$$\Leftrightarrow \quad 2W_h + (\mathcal{Q} N_0)^{-1} = \frac{2W_s}{\pi} \tan(\pi W_h / 2W_s)$$

$$\Leftrightarrow \quad \frac{W_h}{W_s} + (2W_s \mathcal{Q} N_0)^{-1} = \frac{1}{\pi} \tan\left(\frac{\pi}{2} \frac{W_h}{W_s}\right) . \tag{2.101}$$

The above transcendental equation has been numerically solved for various values of $W_s \mathcal{Q} N_0$ and the resulting solution W_h / W_s is plotted in Fig. 2-25. It can be observed that as $W_s \mathcal{Q} N_0$ approaches zero (which results when the detector is "bad" and/or the input noise is negligeable), W_h approaches W_s (the largest it can get). On the other hand, as $W_s \mathcal{Q} N_0$ becomes large (which results from a "good" detector or powerful input noise), W_h approaches $0.742\, W_s$ (the result already found and given in Eq. (2.50)) indicating that emphasis is now on the effect of the input rather than the detector noise.

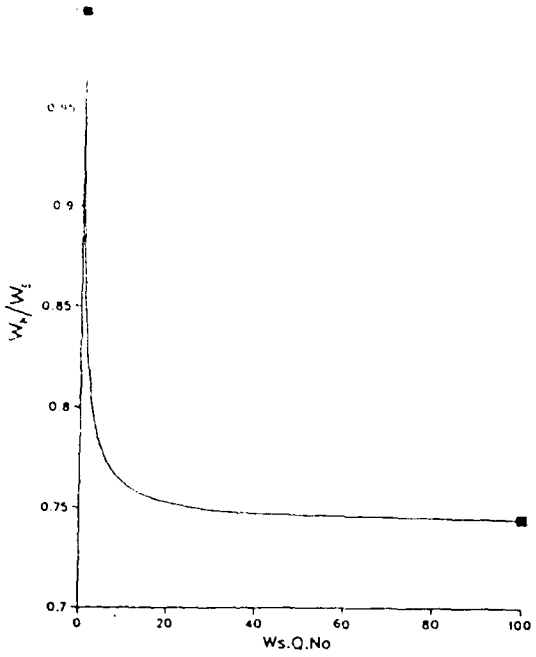

Figure 2-25: Plot of W_h/W_s as a function of $W_s Q N_0$

2.8.4. Realistic 2-D example

In this section, we illustrate the design of OPOF in the presence of detector noise with the help of a 2-D realistic signal. We assume white input noise. With this assumption, the discrete approximation to Eq. (2.96) is given by

$$SNR(K) = \frac{1}{N_0} \frac{\left[\sum_{i=1}^{K} |S(i)|\right]^2}{(Q N_0)^{-1} + K}, \tag{2.102}$$

where in the above equation, we assume that the pixel magnitudes $|S(i)|$, $i = 1,..., d$, have been sorted in descending order.

We have modified our algorithm for support selection to take into account the extra term in Eq. (2.102) due to the detector noise. We have applied the modified algorithm on the tank image shown in Fig. 2-3. As already mentioned, we expect the supports generated to depend on the factor $Q N_0$. The larger its value, the more we weigh the input noise with respect to the detector noise and vice-versa. This is illustrated by Figures 2-26

- 2-28. Figure 2-26 shows the support of the OPOF with $\mathcal{Q}N_0>>1$. As expected, it is the same as in Figure 3, since for large values of QN_0 we tend to ignore the detector noise all together. Figure 2-27 shows the support with $\mathcal{Q}N_0$=0.001. The support size has grown from 59 pixels to 1481 pixels. This larger support allows more input light through to counteract the detector noise. Finally, Figure 2-28 shows the case where $\mathcal{Q}N_0$=10^{-5}. The support has expanded almost to the maximum it can get to, since now the detector is the limiting factor in the system.

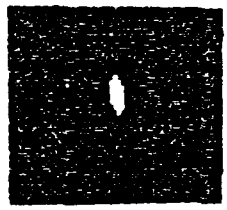

Figure 2-26: OPOF support with $\mathcal{Q}N_0>>1$.

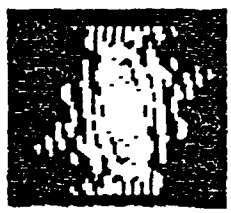

Figure 2-27: OPOF support with $\mathcal{Q}N_0$=0.001.

2.9. Conclusion

In this chapter we investigated ways of designing optimal (in the sense of maximizing the Signal-to-Noise Ratio) phase-only filters (POFs). We introduced the notion of OPOFs which are obtained by determining the phase functions that maximize the resulting SNR. These OPOFs happen to have the same phase functions as the conventional POFs except

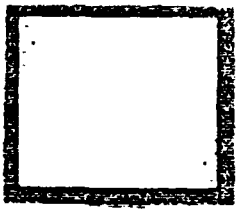

Figure 2-28: OPOF support with $Q N_0 = 10^{-5}$

that their supports must be chosen carefully. While we have not determined the exact nature of the support for arbitrary signal and noise scenarios, we were able to provide some characterizations that should help towards that goal. We were also able to propose a constructive algorithm for the OPOF for the special case of signals corrupted by additive white noise. Some observations about the support allowed us to find a very efficient sub-optimal algorithm for OPOF design. The loss in SNR of this highly efficient algorithm is very negligeable compared with the speed up factor it offers. We illustrated with the help of analytical examples as well as simulation results that the improvement in SNR obtained from the optimal POFs can be significant. The sensitivity of POFs to input distortions relative to OPOFs was also investigated. Our simulation results support the fact that POFs are highly sensitive to distortions, as their performance (in terms of SNR) sharply degraded with input rotations. On the other hand the OPOF seems to exhibit a more robust behavior.

An obvious disadvantage associated with the proposed OPOFs is that the resulting output correlations are broad and thus the resulting accuracy in locating the objects will be poor. This is a direct consequence of the fact that the OPOFs have much lower bandwidths compared to the conventional POFs. However, the larger bandwidths of the conventional POFs allow all the input noise to pass through without any attenuation. Thus, the conventional POF yields lower SNR values, but sharper correlation peaks compared to the proposed OPOFs. Thus, a choice must be made by the user as to which

measure is more relevant to the particular application at hand. The SNR measure is aimed at characterizing the filter performance in the presence of additive noise whereas the correlation peak sharpness is maximized when good location accuracies are required.

Furthermore, the smaller overall support of the OPOFs will also result in less light through-put compared to the conventional POFs. This is probably acceptable for applications where high quality detectors are used. However, if the noise generated in the detectors is not negligeable, or if the light budget in the system is tight, some considerations should be given to the detector noise. This enticed us to investigate designing OPOF in the presence of detector noise. The results we provided in this context turned out to be an interesting generalizing framework for the design of OPOFs. Essentially, they support our previous findings for "good enough" detectors and as their quality degrades, less emphasis is given to the input noise by enlarging the support further.

Chapter 3

Binary Phase-only Filters

3.1. Introduction

The previous chapter focused on the use of Phase-Only Filters (POFs) in optical correlators. POFs are useful since they lead to simpler filters by eliminating the amplitude variations. This constitutes a first step towards achieving *real-time* correlations using the recently introduced Spatial Light Modulators (SLMs)[6, 7, 8] which operate in a phase-only mode. Most of these devices[6, 7, 25], however, function in a *binary* mode, hence requiring the use of Binary Phase-Only Filters (BPOFs). Earlier efforts obtained BPOFs by a simple binarization of POFs. Different binarization schemes were used. Some of these were based on the binarization of the real part[3] of the POF (that we shall denote by $S_r(f)$), some on the imaginary part[10] (denoted $S_i(f)$), and some on their sum[11]. However, there is no obvious reason for choosing one scheme or the other, and this lack of rigorous understanding precluded any consideration of optimality.

Recently, there has been some development of relevance to the design of BPOFs. This has to do with the choice of the Threshold Line Angle (TLA)[26] in constructing the BPOFs. Farn and Goodman[5] proved[xi] that the optimal (in the sense of maximum SNR) BPOF phase assignment is equivalent to optimally selecting the TLA. This basically divides the complex plane into two half-planes such that any phase angle (of the reference signal) falling in one half-plane is quantized to one value and any phase angle falling in the

[xi] However, in their proof, Farn and Goodman[5] missed an important detail. We shall cover this point in a forthcoming section.

other half-plane is assigned the other value. Several research groups[27, 11, 28, 26, 5] seem to have independently realized that the TLA is another variable that can be optimally selected to improve the performance of the BPOF. Furthermore, BPOFs were in most cases constrained to have values of +1 or -1. The justification for this is that some of the SLMs[6] operate with a π phase difference between the two phase values. However, some SLMs (such as the Deformable Mirror Device (DMD)[8]) allow for a much larger dynamic range in phase. This allows the use of more general BPOFs that take on phases ξ or ψ. Farn and Goodman[5] were the first to treat this more general BPOF and optimally solve for ξ and ψ to maximize the SNR.

Nevertheless, all the above approaches still lacked an important ingredient in the design of BPOFs. No attention was given to the the support function which was taken to be arbitrarily large. As argued in the POF case, this could cause the output SNR to be low (possibly zero!). Thus, even though some of the parameters involved in BPOFs have been optimally chosen, the above designs are not *truly optimal (in the sense of maximum* SNR). In this work, we aim at filling this gap by incorporating the support function within the design of BPOFs. While Farn and Goodman[5] have proposed an efficient method for selecting the TLA for a given support, we shall consider the selection of both the TLA and the support simultaneously[xii]. This will allow us to assess the relative effect of these two design parameters on the SNR. We will show through numerical evaluations that choosing the optimal support function seems to increase the SNR by about 4 to 6 dB, whereas choosing the optimal TLA seems to increase the SNR only by about 1 to 2 dB (this confirms earlier[28] theoretical predictions that varying the TLA would not improve the SNR by more than 2 dB).

[xii] With the introduction of the support function in BPOF, the filter is not two-valued any more. It takes on the two phase values (e.g., π and 0) with amplitude 1 as well as the zero amplitude. Thus, it should perhaps be termed the ternary-valued filter or ternary phase-amplitude filter (TPAF)[29].

In this chapter, We shall propose efficient algorithms for the design of the optimal BPOFs. The first is an extension of the algorithm presented in the previous chapter. The second, a very efficient sub-optimal algorithm, is also a generalization of the sub-optimal algorithm presented earlier. Hence, in some sense, this chapter can be regarded as an extension of the previous one. This extension will be clearest when we show that the algorithms of the previous chapter can be applied to the BPOF case after slight modifications. This has the implication that many of the results we obtained with the POF also hold with BPOFs. Thus, the effect of detector noise, the window approximation to the support, etc., all follow directly from the POF case. In an effort to minimize the redundancy, we shall be concerned mainly with the salient design aspects of BPOFs that did not arise while treating POFs. Amongst such aspects is the bifurcation phenomenon[30].

The remainder of this chapter is divided as follows. In Section 2 we provide the analysis necessary to introduce our first algorithm for optimal BPOF design. Section 3 presents some numerical and simulation results using realistic 2-D images. Section 4 outlines a very efficient sub-optimal algorithm. Section 5 is used to show how to cast the BPOF design in the context of the POF. This will help to make use of some of the previous results. Furthermore, we shall provide in that section a more rigorous proof of the main result of Farn and Goodman[5] regarding Optimal BPOFs. In section 6 we investigate the bifurcation issue, characteristic of BPOF. Section 7 presents some computer simulations about the sensitivity of BPOF and Optimal BPOFs to input distortions. Finally we provide a summary in Section 8.

3.2. Efficient Algorithm for Optimal BPOF Design

3.2.1. Analysis

In the following, we assume BPOFs to be constrained to take on the values +1 or -1. The two remaining parameters at hand in the design of BPOFs are the TLA θ and the support. Thus, the BPOF is written as

$$H(f) = \mathrm{I}_{\mathcal{R}} \ \mathrm{Sgn}(S_r(f)\cos(\theta) + S_i(f)\sin(\theta)) \ , \tag{3.1}$$

where $\mathrm{I}_{\mathcal{R}}$ is the indicator function for region $\mathcal{R}$ (the support) and where $\mathrm{Sgn}(x)$ is defined as

$$\mathrm{Sgn}(x) = \begin{cases} +1 & \text{if } x \geq 0 \\ -1 & \text{otherwise} \end{cases} . \tag{3.2}$$

Hence, We now focus on the sign of $(S_r(f)\cos(\theta) + S_i(f)\sin(\theta))$ instead of $S_r(f)$ or $S_i(f)$ alone. Geometrically, this can be described as projecting the complex vector $S(f)$ onto the unit vector with coordinates $(\cos(\theta),\sin(\theta))$ and assigning the sign of the projection to the BPOF. This is illustrated in Figure 3-1. The BPOF form given in Eq. (3.1) unifies all the binarization schemes that have been proposed. Hence, $\theta = 0^\circ$ corresponds to the binarization with respect to the real part[3] of $S(f)$. $\theta = 90^\circ$ corresponds to the binarization with respect to the imaginary part[10], and $\theta = 45^\circ$ to the Hartley transform binarization scheme[11].

Now we seek to find the optimal values for θ and $\mathcal{R}$ to maximize the SNR given by

$$\mathrm{SNR} = \frac{| \int S(f) \ H(f) df |^2}{\int P_n(f) \ | H(f) |^2 \ df} \ , \tag{3.3}$$

where the limits of integration are from $-\infty$ to $+\infty$. The idea is to fix θ and optimize for that choice the SNR with respect to the support $\mathcal{R}$. This process is repeated for all possible

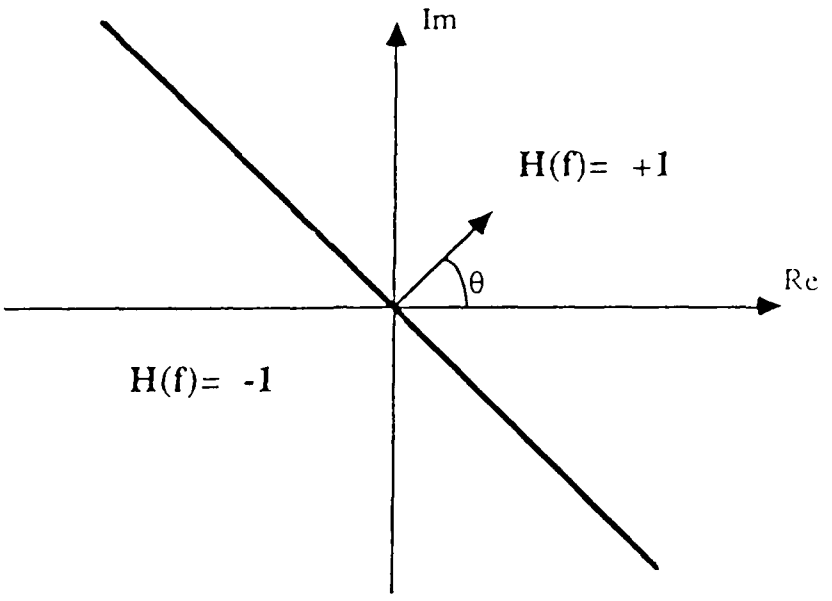

Figure 3-1: General binarization scheme

values of TLA, and the combination of TLA-support that yields the largest SNR is selected. Let θ be fixed. Let us define the partition $(\mathcal{R}_1,\mathcal{R}_2)$ of $\mathcal{R}$ (i.e., $\mathcal{R}_1 \cap \mathcal{R}_2 = \emptyset$ and $\mathcal{R}_1 \cup \mathcal{R}_2 = \mathcal{R}$) as follows:

$$\mathcal{R}_1 = \{ f \in \mathcal{R} : |S_r(f)\cos(\theta)| > |S_i(f)\sin(\theta)| \} \tag{3.4}$$

and

$$\mathcal{R}_2 = \{ f \in \mathcal{R} : |S_r(f)\cos(\theta)| \leq |S_i(f)\sin(\theta)| \} . \tag{3.5}$$

For real $s(x)$, $S_r(f)$ is even symmetric and $S_i(f)$ is odd symmetric. Thus, $\mathcal{R}_1$ and $\mathcal{R}_2$ can be seen to possess even symmetry[xvii]. Using Eq. (3.1) in the SNR expression (Eq. (3.3)) and using the fact that $\mathcal{R}_1$ and $\mathcal{R}_2$ are symmetric, we get

---

[xvii] We are implicitly assuming that $\mathcal{R}$ is even-symmetric, i.e., if a particular spatial frequency f is contained in $\mathcal{R}$, then its negative $-f$ is also contained in $\mathcal{R}$. We can construct counter examples where asymmetric choices for $\mathcal{R}$ yield higher SNR values than the best symmetric choice. However, symmetric $\mathcal{R}$ choices yielded the best SNR whenever $s(x)$ corresponded to a real, positive function. Thus, we believe that (even though we are unable to prove it) for real image correlations we can assume that $\mathcal{R}$ is even-symmetric without loss of optimality.

$$SNR = \frac{\left| \int_{\mathcal{R}_1 \cup \mathcal{R}_2} (S_r(f) + j\,S_i(f))\,\mathrm{Sgn}[S_r(f)\cos(\theta) + S_i(f)\sin(\theta)]\; df \right|^2}{\int_{\mathcal{R}_1 \cup \mathcal{R}_2} P_n(f)\, df}$$

$$= \frac{\left| \int_{\mathcal{R}_1} S_r(f)\,\mathrm{Sgn}[S_r(f)\cos(\theta)]\, df + j \int_{\mathcal{R}_2} S_i(f)\,\mathrm{Sgn}[S_i(f)\sin(\theta)]\, df \right|^2}{\int_{\mathcal{R}_1 \cup \mathcal{R}_2} P_n(f)\, df}$$

$$= \frac{\left| \mathrm{Sgn}[\cos(\theta)] \int_{\mathcal{R}_1} |S_r(f)|\, df + j\,\mathrm{Sgn}[\sin(\theta)] \int_{\mathcal{R}_2} |S_i(f)|\, df \right|^2}{\int_{\mathcal{R}_1 \cup \mathcal{R}_2} P_n(f)\, df}$$

$$= \frac{\left[\int_{\mathcal{R}_1} |S_r(f)|\, df\right]^2 + \left[\int_{\mathcal{R}_2} |S_i(f)|\, df\right]^2}{\int_{\mathcal{R}_1 \cup \mathcal{R}_2} P_n(f)\, df} . \qquad (3.6)$$

In the above we made use of the fact that $\mathrm{Sgn}\,(A+B) = \mathrm{Sgn}\,(A)$ whenever $|A| > |B|$. Let us note that θ need not be outside the range $[0,\pi/2]$. First, from Eq. (3.1), if $H(f)$ is obtained using angle θ and if $H'(f)$ is obtained using $\theta' = \theta+\pi$, then

$$H'(f) = -H(f) . \qquad (3.7)$$

This scaling does not affect the SNR and can be ignored. Furthermore, from Eq. (3.6), it is observed that the only way θ affects the SNR is through the partition $(\mathcal{R}_1,\mathcal{R}_2)$. Again, by looking at Eqs. (3.4), (3.5), we conclude that angles θ and $\theta'' = \pi - \theta$ will yield the same regions $\mathcal{R}_1$, $\mathcal{R}_2$. Hence, we only need to consider values of θ in the range $[0,\pi/2]$.

It turns out that we can apply the same idea (in the discrete domain) as in the OPOF case for white noise to find an efficient way of optimizing the SNR in Eq. (3.6). For a given θ, we define the two regions

$$P_1 = \{ i : |S_r(i)\cos(\theta)| > |S_i(i)\sin(\theta)| \} \tag{3.8}$$

and

$$P_2 = \{ i : |S_r(i)\cos(\theta)| \leq |S_i(i)\sin(\theta)| \} . \tag{3.9}$$

The values $|S_r(i)|$ for $i \in P_1$ and the values $|S_i(i)|$ for $i \in P_2$ are then sorted in descending order. Hence, a discrete approximation for Eq. (3.6) is

$$SNR = \frac{\left[\sum_{i=1}^{K_1} |S_r^i|\right]^2 + \left[\sum_{i=1}^{K_2} |S_i^i|\right]^2}{K_1 + K_2} , \tag{3.10}$$

where K_1 and K_2 denote the number of pixels in P_1 and P_2, respectively. Here the superscript i in $|S_r^i|$ and $|S_i^i|$ refers to the ith largest value in the corresponding array.

Now, we need to find the optimal values of K_1, K_2 through a search along the grid (i.e., we fix K_1 and find the optimal value of K_2 and repeat this process for all values of K_1 and choose the best case). The next section presents the details of this optimization algorithm.

3.2.2. Algorithm

STEP 0: Determine P_1 and P_2 according to Eqs. (3.8) (3.9). Let N_1 and N_2 denote the number of pixels in P_1 and P_2, respectively. Without loss of generality, assume that $N_2 \leq N_1$.

STEP 1: Arrange $|S_r(m)|$ for $m \in P_1$ and $|S_i(m)|$ for $m \in P_2$ in the following order.

$$|S_r^1| \geq |S_r^2| \geq \cdots \geq |S_r^i| \cdots \geq |S_r^{N_1}| ,$$
$$|S_i^1| \geq |S_i^2| \geq \cdots \geq |S_i^i| \cdots \geq |S_i^{N_2}| . \tag{3.11}$$

Set all parameters such as k_1, k_2, k_1^{OPT}, k_2^{OPT}, SNR_{MAX}, RESUM

(real-part running sum) and IMSUM (imaginary-part running sum) to zero.

STEP 2: $k_1 \rightarrow k_1 + 1$

RESUM $\rightarrow$ RESUM $+ |S_r^{k_1}|$

SNR $(k_1,k_2) = [(\text{RESUM})^2 + (\text{IMSUM})^2]/(k_1+k_2)$

If SNR $(k_1,k_2) \geq$ SNR $_{MAX}$, SNR $_{MAX}$ = SNR (k_1,k_2),

$$k_1^{\text{OPT}} = k_1 \text{ and } k_2^{\text{OPT}} = k_2.$$

Otherwise, no changes.

STEP 3: If $k_1 < N_1$, go to Step 2.
Otherwise, $k_2 \rightarrow (k_2+1)$.
If $k_2 > N_2$, go to Step 4.
Otherwise, RESUM $= 0$, $k_1 = 0$, IMSUM $=$ IMSUM $+ |S_i^{k_2}|$
Go to Step 2.

STEP 4: Output k_1^{OPT}, k_2^{OPT} and SNR $_{MAX}$. Knowing k_1^{OPT} and k_2^{OPT} defines the optimal support uniquely.

The above steps are repeated for all possible values of TLA θ, and the case leading to the best SNR is selected. Numerical evaluations illustrating the resultant performance improvement by applying the above algorithm are presented in the next section.

3.3. Numerical Results

To illustrate the improvements possible with the optimal BPOF, we performed numerical experiments using the same 32×32 tank image used previously. This image was placed in a 64×64 array and zero-padded to reduce sampling effects. The center of the tank image was made to coincide with the origin of the 64×64 array. As pointed out by Cottrell et. al.[11], the performance of BPOF is a strong function of the image center and we ensured that the image is centered at the origin. This image has an energy of 73860 in its even part and 48708 in its odd part. This corresponds to a total image energy of 122568.

Assuming the white noise variance N_0 to be 1, this represents a Matched Filter (MF) SNR equal to 122568 or 50.88 dB.

Next, we performed the 64×64 2D Fast Fourier Transform (FFT) on the array and used the efficient algorithm outlined in the previous section to identify the optimal P_1 and P_2 for several θ values. We also computed the resulting optimal $\mathrm{SNR}_{BPOF}^{OPT}$, the Horner efficiency[6] for the optimized BPOF and SNR_{BPOF} obtained by using a BPOF whose support is the entire 64×64 array. The SNR values are shown in Fig. 3-2 as a function of the Threshold Line Angle. Note from Fig. 3-2 that all BPOF SNRs are lower than the

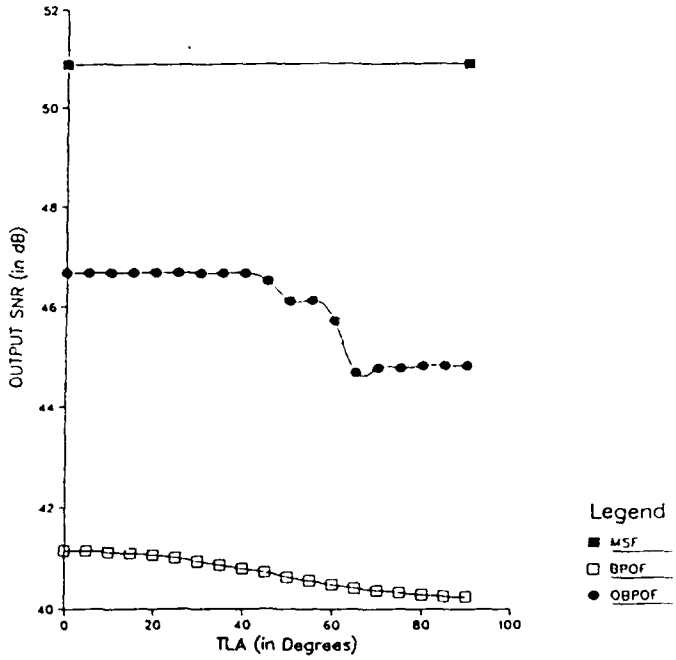

Figure 3-2: Output SNR (vs) TLA for BPOF and Optimal BPOF for centered tank.

50.88 dB provided by the classical MF. The unoptimized BPOF yields SNR values ranging from 40.25 dB (for $\theta = 90^\circ$) to 41.15 dB (for $\theta = 0^\circ$). This represents a degradation of about 10 dB in SNR. On the other hand, the optimized BPOF yields SNR values ranging from 44.68 dB (for $\theta = 65^\circ$) to 46.68 dB (for $\theta = 0^\circ$). This represents a degradation in SNR from 4.2 dB to 6.2 dB compared to the matched filter. Thus an SNR improvement of

5 dB can be obtained (for the particular cases studied) by selecting the support function of the BPOF in an optimal manner . This observation seems to be true for essentially all θ values.

In Fig. 3-3(a)-3-3(c), we show the optimal support function for $\theta = 0^\circ$ (33 pixels "ON"), $\theta = 60^\circ$ (19 pixels "ON"), and $\theta = 90^\circ$ (58 pixels "ON"), respectively. In

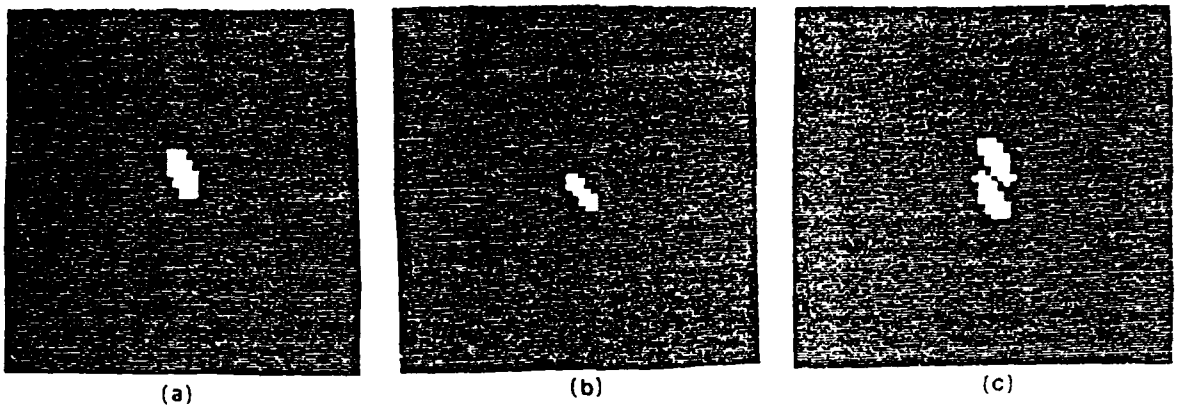

Figure 3-3: Optimal supports for $\theta = 0^\circ$, 60°, 90° using centered tank.

particular, note the two unconnected regions in Fig. 3-3(c) for the support function. In Fig. 3-4, we show the Horner light efficiency of optimal BPOFs as a function of the Threshold Line Angle. Note from Figs. 3-2 and 3-4 that the Horner efficiency of the optimized BPOFs exhibits more fluctuations than the SNR as the TLA varies, changing between 56.6% (for $\theta = 90^\circ$) and 35.9% (for $\theta = 60^\circ$). It is interesting to note that as θ gradually changes from 0° to 60°, both $\mathrm{SNR}_{BPOF}^{OPT}$ and Horner efficiency keep decreasing. Hence, in this regard, $\theta = 60^\circ$ could be considered as a "worst case" TLA.

As already mentioned, the performance of BPOFs strongly depends on the position of the reference image in the FFT array at the time the filter is synthesized. In the above results, the tank has been centered in the FFT array. To investigate the effect of moving the reference image around, we positioned the tank in the upper left corner of the 64 by 64 FFT array. The energy in the even and odd part became both equal to 61283.9. This is to be expected, since the flipped version of the tank now has no overlap with the tank image itself. The numerical results in this case are summarized in Figs. 3-5 and 3-6 which are the

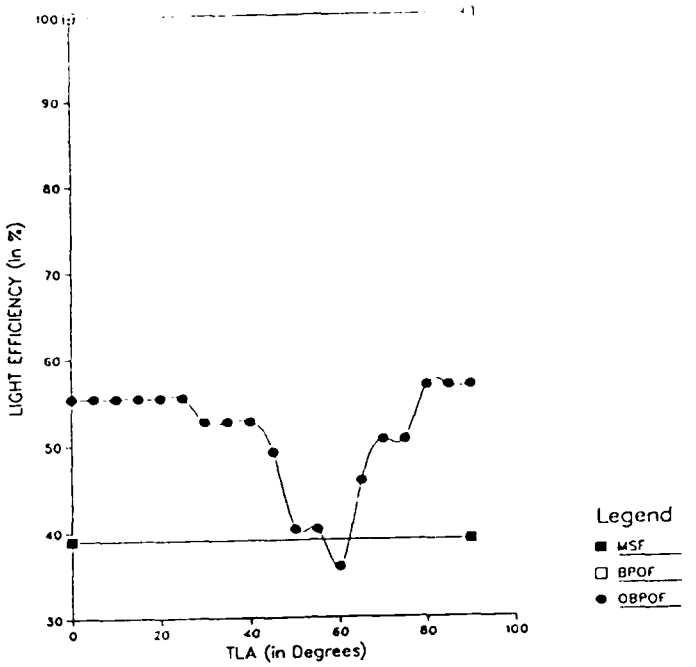

Figure 3-4: Horner light efficiency (vs) TLA for centered tank.

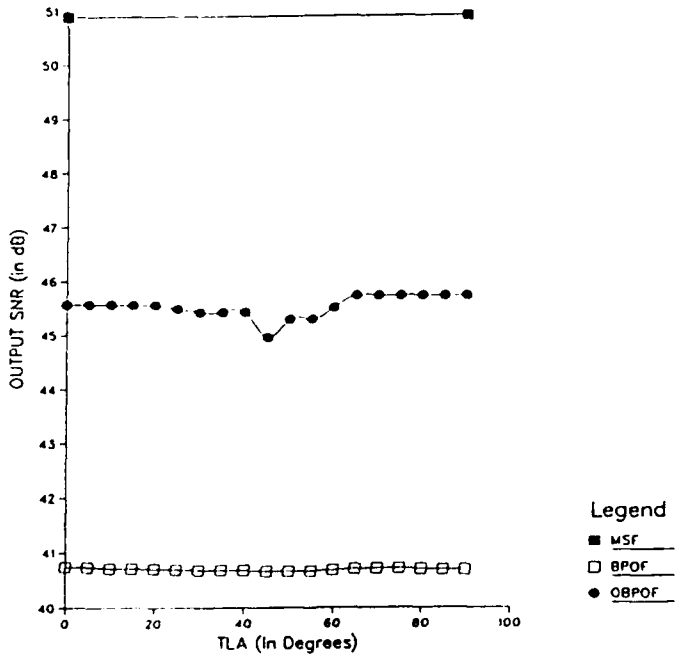

Figure 3-5: Output SNR (vs) TLA for BPOF and Optimal BPOF for non-centered tank.

counterparts of Figs. 3-2 and 3-4, respectively. The most noticeable change is the fact that the output SNR for both BPOF and OBPOF corresponding for TLAs greater than 45 have now increased. Actually, this happened even to the extent that the OBPOF(im) now yields the highest output SNR. This is a direct consequence that we have given more weight to

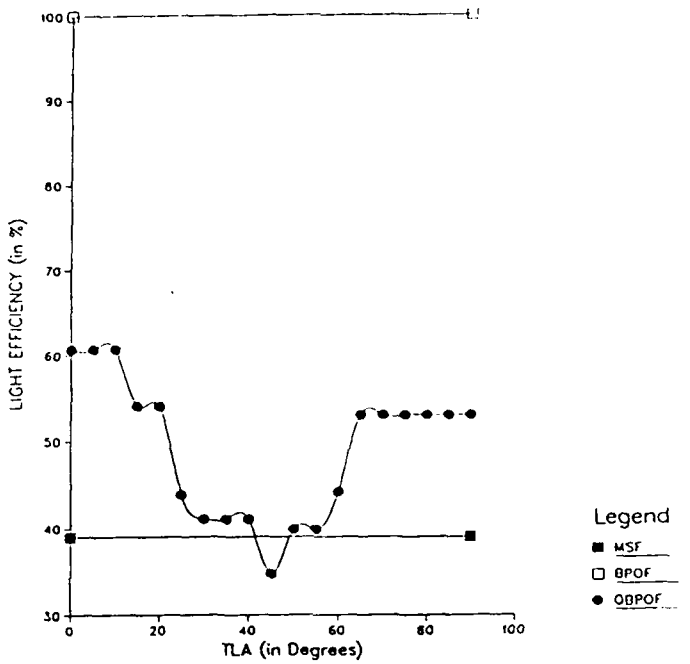

Figure 3-6: Horner light efficiency (vs) TLA for non-centered tank.

the imaginary part of $S(f)$ by redistributing the signal energy more evenly.

All the results presented above are based on numerically evaluating the SNR in Eq. (3.10). Some simulations were carried out on the same tank image. Six filters were used: the BPOF and optimized BPOF corresponding to $\theta = 0^\circ, 45^\circ, 90^\circ$. These filters are the same as those used in our numerical computation of SNRs with the tank centered in the FFT array. We obtained an estimate of output SNRs with all six filters by adding zero-mean, unit variance Gaussian noise to the tank image. Next, the corrupted image is padded with zeros, and a 64 by 64 FFT is computed. The correlation outputs at the origin are then recorded. This process is repeated 100 times and estimates of SNRs are computed

through averaging. Fig. 3-7 depicts the output SNR as a function of input SNR for the BPOFs corresponding to $\theta = 0^\circ$ (this case is denoted by BPOF(re)), $\theta = 45^\circ$ (denoted BPOF(ha)), and $\theta = 90^\circ$ (denoted BPOF(im)). Even though the three curves are close together, a hierarchy can be observed wherein the BPOF(re) yields the highest SNR followed by BPOF(ha), and finally by BPOF(im). This is in agreement with the numerical evaluations presented in Fig. 3-2. Fig. 3-8 is analogous to Fig. 3-7 except we use the

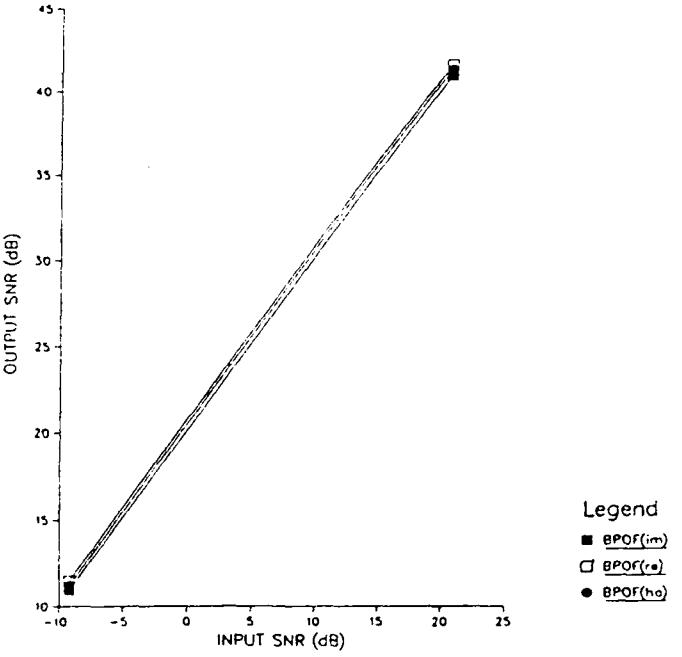

Figure 3-7: Output SNR (vs) input SNR for BPOF(re), BPOF(ha), and BPOF(im) using centered tank.

Optimal BPOFs instead. It can be seen that the support optimization provided an improvement in SNR by 5 to 6 dB. Furthermore, the OBPOF(re) yielded an SNR slightly higher than the OBPOF(ha). The output SNR of the OBPOF(im) is noticeably below both that of the other two filters. In addition, we noticed that the output SNR (in all cases) corresponding to an input noise variance of 1 (i.e., a 0 dB input SNR) are all within 1.4 dB from the numerically computed values. Table 3-1 summarizes our results. Moreover, as an illustration, Fig. 3-9 depicts the output SNR of BPOF(re) and OBPOF(re) in reference

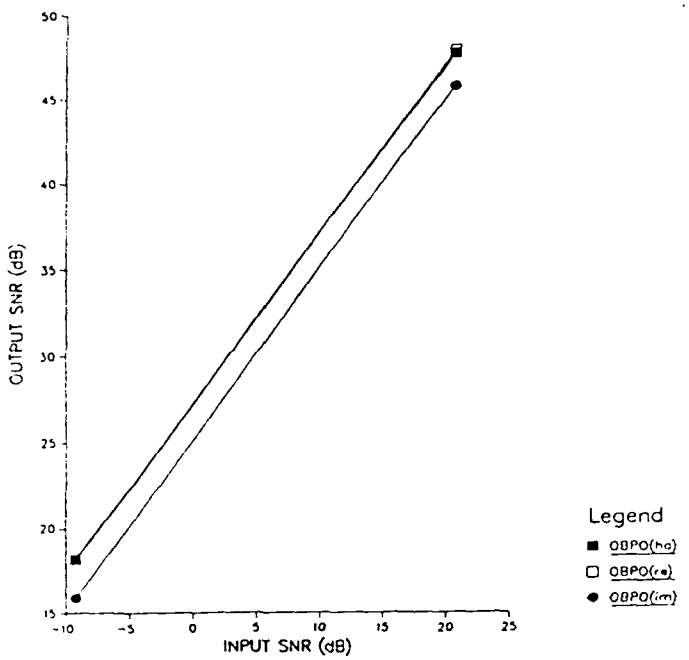

Figure 3-8: Output SNR (vs) input SNR for OBPOF(re), OBPOF(ha), and OBPOF(im) using centered tank.

Output SNR(dB)

	Simulation		Numerical	
	BPOF	OBPOF	BPOF	OBPOF
θ=0	41.68	48.05	41.15	46.68
θ=45	41.4	47.85	40.72	46.51
θ=90	41.0	45.88	40.25	44.82

Table 3-1: Simulation (vs) numerical results BPOFs and OBPOFs using tank image.

to the MSF, POF, and OPOF found in the previous chapter. A clear hierarchy can be observed. First, and as expected, the MSF has the highest SNR followed by the OPOF

(with 1.5 dB less SNR). Next is the Optimal BPOF with about 3 dB less SNR than the MSF followed by the POF with a degradation of the order of 5 dB. At the lowest rank is the BPOF with an output SNR approximately 10 dB lower than the MSF and 5 dB lower than the POF. This last result is within the maximum 6 dB drop in SNR due to binarization predicted by Dickey et al.[23].

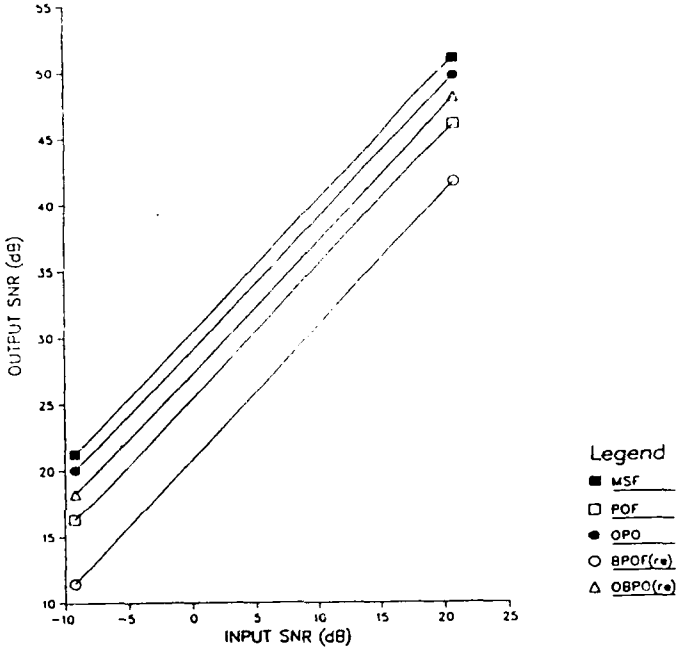

Figure 3-9: Output SNR (vs) input SNR for
MSF, POF, OPOF, BPOF(re), and OBPOF(re) using centered tank.

All the above numerical evaluations and simulation results were carried out for the pliers image presented in the previous chapters. The improvement in SNR due to the support optimization varied from 2 to 4 dB. All simulations were also within 1.2 dB from the numerically computed SNRs. Furthermore, almost all of the observations and trends discussed for the tank image apply to the pliers. Namely, the SNR again showed little variations with respect to the TLA (less than 0.5 dB for BPOF and about 2 dB for OBPOF). Also, the Horner light efficiency exhibited more variations than the SNR. The variations in this case, however, are more noticeable than for the tank image and are

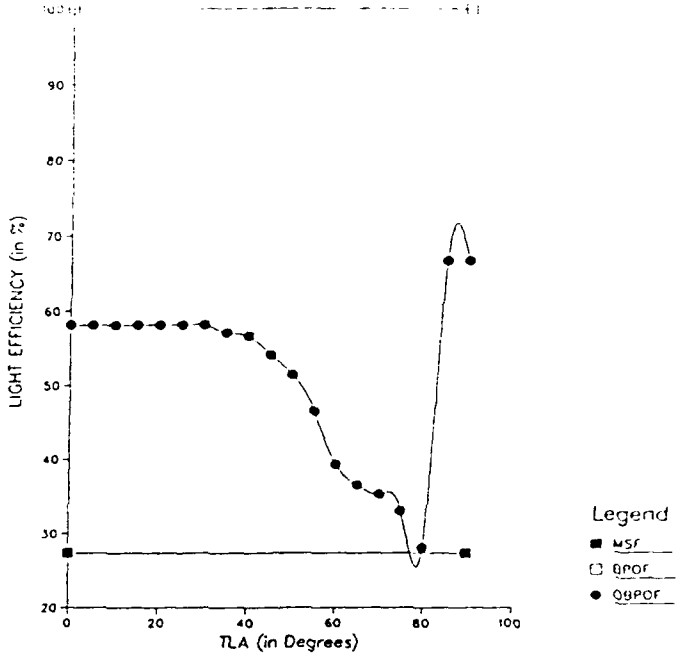

Figure 3-10: Horner light efficiency (vs) TLA for centered pliers.

shown in Fig. 3-10. Notice the large jump for TLAs equal to 85 and 90 degrees. The rest of the data and results are rather similar to the tank example. We omit their presentation for the sake of conciseness.

It can be seen from the above discussion that the TLA and support function offer two degrees of freedom in the design of BPOFs. If light efficiency is not a problem (for example in applications where ample light is available), it is recommended that we invest our computational resources in the optimization of the support function, assuming $\theta = 0^\circ$. The justification for this is that SNR showed a relatively small variation (for the particular cases studied) with respect to the TLA (about 2 dB for the optimized BPOF and about 1 dB for the unoptimized BPOF) along with the fact that most images are even-part dominated. Our simulation results further support this argument ($\theta = 0^\circ$ yields the best SNR and an acceptable light efficiency level). If on the other hand light is at a premium, then more attention should be given to the TLA. For instance, $\theta = 90^\circ$ with

the pliers image seems to be a plausible solution since it has the highest Horner efficiency at the expense of only a 2 dB degradation in SNR.

3.4. Very Efficient Sub-Optimal Algorithm for BPOF Support Optimization

3.4.1. Analysis

We base this very efficient algorithm on the observation summarized in the following proposition.

Proposition 1: If the real (imaginary) part of two or more pixels in $\mathcal{P}_1$ ($\mathcal{P}_2$) are equal in absolute value, they are either or none included in the optimal $\mathcal{P}_1$ ($\mathcal{P}_2$).

Proof: The proof is very similar to that of the corresponding proposition in the previous chapter. The only difference is that the optimization is now performed on a grid. Hence, the only thing that needs to be checked is that by replacing the discrete version of the SNR expression (given in Eq. (2.65)) by

$$SNR^{\sim}(k) = \frac{(\sum_{i=1}^{k} |S(i)|)^2 + a}{k + b}, \tag{3.12}$$

where a and b are *arbitrary* non-negative constants, the conclusion of the first part of the proof of proposition (3) in the previous chapter is unaffected. Namely, it can be established in exactly the same way as before that if $|S(k_o)| = |S(k_o+1)|$ for some $k_o \geq 2$ and if $SNR^{\sim}(k_o) \geq SNR^{\sim}(k_o-1)$, then $SNR^{\sim}(k_o+1) \geq SNR^{\sim}(k_o)$ •

As before, the idea is to quantize $|S_r(i)|$, $i \in \mathcal{P}_1$ and $|S_i(i)|$, $i \in \mathcal{P}_2$. By virtue of the above proposition, instead of performing the optimization over the $K_1 \times K_2$ grid of pixels (K_1 (K_2) is the total number of pixels in $\mathcal{P}_1$ ($\mathcal{P}_2$)), we focus only on a $N \times N$ grid (N is the quantization level). In the following, we outline the steps of the algorithm.

3.4.2. Algorithm

Below, we roughly list the steps of the efficient sub-optimal algorithm. The details are left out since they have been already presented in one way or the other.

STEP 1: Find the partitions P_1 and P_2.
$M1 = \text{Max} \{ |S_r(i)| , i \in P_1 \}$
$M2 = \text{Max} \{ |S_i(i)| , i \in P_2 \}$
$M = \text{Max}[M1, M2|$
$S(i) \leftarrow S(i)/M , \quad i = 1, ..., d.$

STEP 2: Quantize $|S_r(i)| , i \in P_1$ and $|S_i(i)| , i \in P_2$. Assign tags to the corresponding pixels.

STEP 3: Search through an $N \times N$ grid to get optimal levels L_1 and L_2.

STEP 4: Get optimal P_1 (P_2) by direct comparison with L_1 (L_2).

STEP 5: End.

Note that this grid optimization will increase the computation time by a factor of N over that of the 1-D algorithm presented earlier. Yet, we will see shortly how to adapt the BPOF problem to the POF algorithm. Hence, this will result in the most efficient technique for OBPOF design. The only shortcoming of that approach (as we will see) is that only the optimal (in the sense of maximum SNR) TLA solution will be generated. The SNR for other TLAs as well as the Horner light efficiency will not be correctly computed. This is what motivated the introduction of the above two algorithms for OBPOF design. More will be said about this later.

3.4.3. Numerical Results

We have implemented and tested the above algorithm. Using the same 32 by 32 tank image and a 64 by 64 (the tank has been centered) FFT, it took 1585 seconds to find the optimal support functions for the 19 BPOFs (corresponding to the 19 TLAs, from 0 to 90 in increments of 5 degrees) using the old "improved"[xiv] algorithm. Applying the new algorithm with $N = 256$, it took only 16.8 seconds to obtain 18 supports exactly and one support within 2 pixels (60 instead of 58 pixels). The time reduction factor is about 95. By increasing N to 400, all the supports were computed correctly in 36.4 seconds. This lead to a reduction factor of 44. It can be seen from here that the computing time of the new algorithm is a faster increasing function of N than in the OPOF case. This is a direct consequence of the search over a grid.

As before, we anticipate that the time reduction factor becomes more noticeable as the number of pixels increases. We increased the FFT size to 128×128 and focused on the optimal support for the Hartley BPOF (TLA = 45 Degrees)[xv]. It took 1939 seconds for the old algorithm to find the optimal support, whereas the new algorithm with $N = 256$ took only 1.98 sec to find the exact answer. This is a reduction factor of about 980!

We performed some more testing on other cases (such as non-centered tank, centered and non-centered pliers) with 64×64 size FFTs. For $N = 256$, 56 out of the 77 supports were found exactly with an average reduction factor in CPU time of about 77. It is interesting to notice that out of the 21 errors made, 17 were committed on the pliers (13 of them on the non-centered case) and only 4 on the tank image. More generally, it was observed that the non-centered cases (i.e., in which the energy in $S(f)$ is almost equally distributed between the even and odd parts of $s(x)$) caused the largest number of errors. Of all these 21 errors, the worst (with the non-centered pliers, $\theta = 90^\circ$) caused a loss of

---

[xiv] By using the Heap sort algorithm.

[xv] Notice that this will lead to conservative results since the sorting time is smallest as the difference in the number of pixels of P_1 and P_2 becomes smaller.

0.00046 dB in SNR. Interestingly, this case turned out to be the most "ill" since it required N as high as 6000 to get the exact answer (in about 301 sec.) This suggests another enhancement to the new algorithm where we adapt N to the data (dynamic range, smallest difference between pixels...etc.). For $N = 400$, 64 out of the 77 supports were exactly found with an average reduction factor of about 35. The worst loss in SNR was well within that of the case with $N = 256$. Once again, all the above timing estimates were done excluding FFTs, inputs/outputs, partitioning and normalization.

3.5. Relating Optimal Designs of BPOFs and POFs

In this section, we establish a link between the optimal design of BPOFs and POFs. We will show that the OPOF algorithm can be used for BPOF design. This will allow us to make use of some of the available results related to the POF support optimization. Thus, the issue of detector noise effect on the support function as well as the window approximation for the support follow directly from the previous chapter. More importantly, this link will provide us with yet another very efficient algorithm for optimal BPOF design. Actually, this third algorithm is the most efficient of all since it does not perform the support optimization over a grid. However, as we shall shortly see, the information it generates (BPOF along with its optimized support, SNR and light efficiency) is relevant only for the optimal TLA. If the variations of SNR and light efficiency as a function of TLA is desired, one of the other two algorithms needs to be used.

Recall that our objective is to find the BPOF $H(f)$ that maximizes the SNR expression given in Eq. 3-3. We shall assume for now that the support R is fixed. Using the fact that the modulus of $H(f)$ equals one for all frequencies, maximizing the SNR becomes equivalent to maximizing the magnitude of the numerator of Eq. (3.3) rewritten as

$$c = \int_{\mathcal{R}} S(f)\, H(f)\, df = |c|\, e^{j\theta} \ . \tag{3.13}$$

Thus, the quantity to be maximized $|c|$ is given by

$$\begin{aligned} |c| \quad &= \int_{\mathcal{R}} S(f)\, e^{-j\theta}\, H(f)\, df \\ &= \int_{\mathcal{R}} S^{\theta}(f)\, H(f)\, df \\ &= \int_{\mathcal{R}} S_r^{\theta}(f)\, H(f)\, df \ + \ j \int_{\mathcal{R}} S_i^{\theta}(f)\, H(f)\, df \\ &= \int_{\mathcal{R}} S_r^{\theta}(f)\, H(f)\, df \ , \end{aligned} \tag{3.14}$$

where $S^{\theta}(f)$ is given by

$$\begin{aligned} S^{\theta}(f) \quad &= S(f)\, e^{-j\theta} \\ &= [S_r(f)\, \cos(\theta) \ + \ S_i(f)\, \sin(\theta)] \\ &\quad + \ j\,[S_i(f)\, \cos(\theta) \ - \ S_r(f)\, \sin(\theta)] \ . \end{aligned} \tag{3.15}$$

It can be seen from Eq. (3.14) that the optimal BPOF is given by

$$\begin{aligned} H_{\theta}(f) \quad &= I_{\mathcal{R}}(f)\, \mathrm{Sgn}\,[S_r^{\theta}(f)] \\ &= I_{\mathcal{R}}(f)\ \mathrm{Sgn}\,[S_r(f)\, \cos(\theta) \ + \ S_i(f)\, \sin(\theta)] \ . \end{aligned} \tag{3.16}$$

Eq. (3.16) can be recognized to be identical to Eq. (3.1), and hence the argument θ can be looked at as the TLA. The resulting maximum value of $|c|$ (function of $\mathcal{R}$ and θ) is given by

$$|c|_m^{\theta} = \int_{\mathcal{R}} |S_r^{\theta}(f)|\, df \ . \tag{3.17}$$

However, we have overlooked an important point in the above analysis. We must ensure

that $H_\theta(f)$ given in Eq. (3.16) will yield the argument θ when used in Eq. (3.13). Actually, this is not true in general and the maximum given in Eq. (3.17) is only an upper bound for $|c|$ with all BPOF leading to an argument of θ. This can be easily seen by applying the fundamental integral inequality to Eq. (3.14). It turns out that this upper bound is achieved by the optimal BPOF $H^*(f)$ (it is optimal amongst all those BPOFs with support equal to $\mathcal{R}$. This $\mathcal{R}$ still needs to be determined) at the argument θ^* it induces in Eq. (3.13). In other words, the condition that the filter $H_\theta(f)$ in Eq. (3.16) induces the angle θ when used in Eq. (3.13) is satisfied for $\theta = \theta^*$. This will be the subject of the following proposition.

Proposition 2: Let $H^*(f)$ be the BPOF that leads to the highest SNR amongst all BPOFs with support $\mathcal{R}$[xvi]. Let θ^* be the argument it induces when used in Eq. (3.13). Then,

$$H^*(f) = H_{\theta^*}(f) \ , \tag{3.18}$$

where, $H_{\theta^*}(f)$ is given by Eq. (3.16).

Proof: [xvii] First, if the filter $H_{\theta^*}(f)$ leads to the angle θ^*, then Eq. (3.18) follows immediately from the above analysis. Let us now assume $H_{\theta^*}(f)$ induces an angle $\omega \neq \theta^*$. By hypothesis, the maximum possible value of $|c|$ is given by

$$\begin{aligned} |c|_M &= e^{-j\theta^*} \int_{\mathcal{R}} S(f)\, H^*(f)\, df \\ &= \int_{\mathcal{R}} S_r^{\theta^*}(f)\, H^*(f)\, df \ \leq \ \int_{\mathcal{R}} |S_r^{\theta^*}(f)|\, df. \end{aligned} \tag{3.19}$$

Now using H_{θ^*} given by Eq. (3.16) in Eq. (3.13), we get

[xvi] In other words, $H^*(f)$ leads to the largest magnitude of the integral in Eq. (3.13).

[xvii] We acknowledge Fred Dickey et al. of Sandia Laboratories for pointing out an important detail in this proof.

$$|c| = e^{-j\omega} \int_{\mathcal{R}} S(f)\ \mathrm{Sgn}\,[S_r^{\theta^*}(f)]\, df$$

$$= e^{-j(\omega-\theta^*)} \int_{\mathcal{R}} S(f)\, e^{-j\theta^*}\ \mathrm{Sgn}\,[S_r^{\theta^*}(f)]\, df$$

$$= e^{-j(\omega-\theta^*)} \int_{\mathcal{R}} [S_r^{\theta^*}(f) + jS_i^{\theta^*}(f)]\ \mathrm{Sgn}\,[S_r^{\theta^*}(f)]\, df\ . \tag{3.20}$$

Taking the magnitude of both terms in Eq. (3.20), we obtain

$$|c| = \left[\left(\int_{\mathcal{R}} |S_r^{\theta^*}(f)|\, df \right)^2 + \left(\int_{\mathcal{R}} S_i^{\theta^*}(f)\ \mathrm{Sgn}\,[S_r^{\theta^*}(f)]\, df \right)^2 \right]^{1/2}$$

$$> \int_{\mathcal{R}} |S_r^{\theta^*}(f)|\, df \ \geq\ |c|_{Af}\ . \tag{3.21}$$

Absurd .

In the above, the strict inequality follows from the assumption that $\omega \neq \theta^*$.[xviii] Thus the assumption that $\omega \neq \theta^*$ does not hold, and the result in Eq. (3.18) follows •

The next step is to maximize with respect to the support $\mathcal{R}$ the SNR resultant from using $H_{\theta^*}(f)$ and given by

$$SNR = \frac{\left[\int_{\mathcal{R}} |S_r^{\theta^*}(f)|\, df \right]^2}{\int_{\mathcal{R}} P_n(f)\, df}\ . \tag{3.22}$$

Eq. (3.22) is very similar to Eq. (2.11) found in the previous chapter. The only difference is that we are now using $|S_r^{\theta^*}(f)|$ instead of $|S(f)|$. This suggests the following very efficient algorithm for OBPOF design based on the techniques used for the OPOF case.

[xviii] Indeed, the equality happens if and only if the second term in the first line of Eq. (3.21) is zero. This in turns happens if and only if the argument of the integral in Eq. (3.13) ($=\omega$) equals θ^*.

STEP 0: $\theta = -\Delta\theta$; $\text{SNR}_{max} = 0$.

STEP 1: $\theta = \theta + \Delta\theta$.

STEP 2: Obtain $|S_r^{\theta}(f)| = |\text{Re}[S(f)\, e^{-j\theta}]|$.

STEP 3: Apply the OPOF algorithm using $|S_r^{\theta}(f)|$ instead of $|S(f)|$. Get corresponding support $\mathcal{R}_o$. Compute corresponding SNR. If greater than SNR_{max} then,

$$\text{SNR}_{max} = \text{SNR}; \quad \theta^* = \theta; \quad \mathcal{R}^* = \mathcal{R}_o.$$

STEP 4: If $\theta \leq \theta_{max}$ go to STEP 1.

STEP 5: End.

The idea in the above algorithm is to scan all possible values of the TLA θ. Each time, $|S(f)|$ is replaced by $|S_r^{\theta}(f)|$ and the OPOF algorithm is applied to optimize the support of $H_{\theta}(f)$. Note, however, that the computed SNR, support function, and light efficiency will not be correct in general (unless $\theta = \theta^*$). Eventually, $\theta = \theta^*$ and we solve for the optimal support, SNR, and light efficiency of $H_{\theta^*}(f)$ (the OBPOF).

We tested this third algorithm on the same images (tank and pliers) we used previously. The optimal BPOFs solved for agree with those found using the other two algorithms. Hence, the optimal TLA is 0 degree for both images when they were centered in the FFT array, and 90 degrees for both when they were placed at the upper left corner. It took around 200 seconds for the third algorithm (using the OPOF algorithm described in the previous chapter) to generate the OBPOF versus the 1585 seconds required by the first algorithm. This is a factor of about 8 reduction in CPU time. However, as already mentioned, we disregarded any information related to all other TLAs but the optimal one. Note that in this case we do not need to make the assumption that $\mathcal{R}$ is even symmetric.

3.6. Bifurcation Issue

The bifurcation phenomenon[13, 20, 23] is one of the most distinctive characteristics of BPOF-design. The most important factor affecting this phenomenon is the symmetry of $S(f)$ at the time the BPOFs are synthesized. This symmetry strongly depends on the position of the reference image in the FFT array. To illustrate this we computed the BPOF and OBPOF using the real part of $S(f)$ in two cases. In the first, the tank image was placed at the upper left corner of the FFT array and in the second it has been centered. For better display, we decided to use 128 by 128 FFTs. Fig. 3-11 plots the correlation of the tank image with the BPOF synthesized from the non-centered tank. The

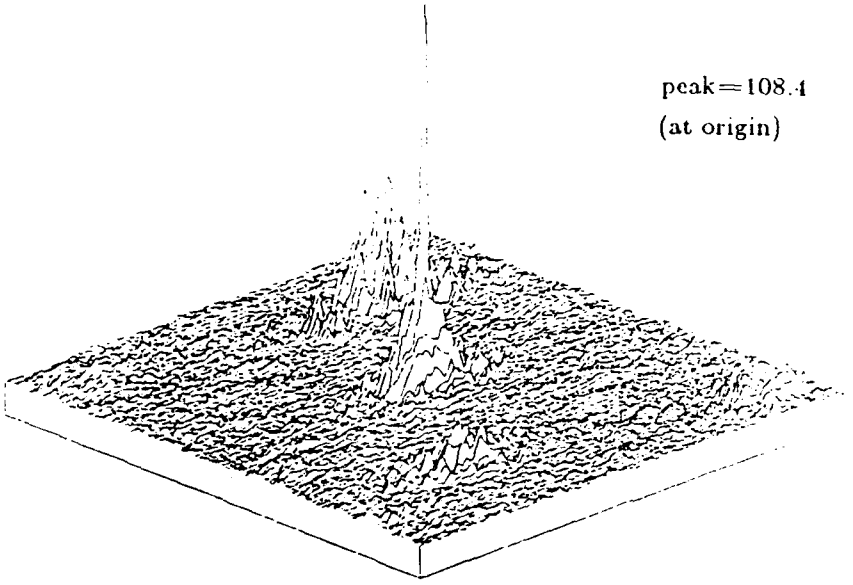

Figure 3-11: Correlation of tank with BPOF(re) in the non-centered case.

existence of a second but smaller peak is noticeable. Actually, the peak corresponds to the autocorrelation of the tank. The second peak is the autoconvolution. Fig. 3-12 is the counterpart of Fig. 3-11 using the OBPOF instead. It can be observed that the second peak became more noticeable (actually it became as large as the peak itself). Also, due to the low pass nature of the support, both peaks have been smoothed. We repeated both correlations with the tank centered at the time the filters are generated. Figs. 3-13 and

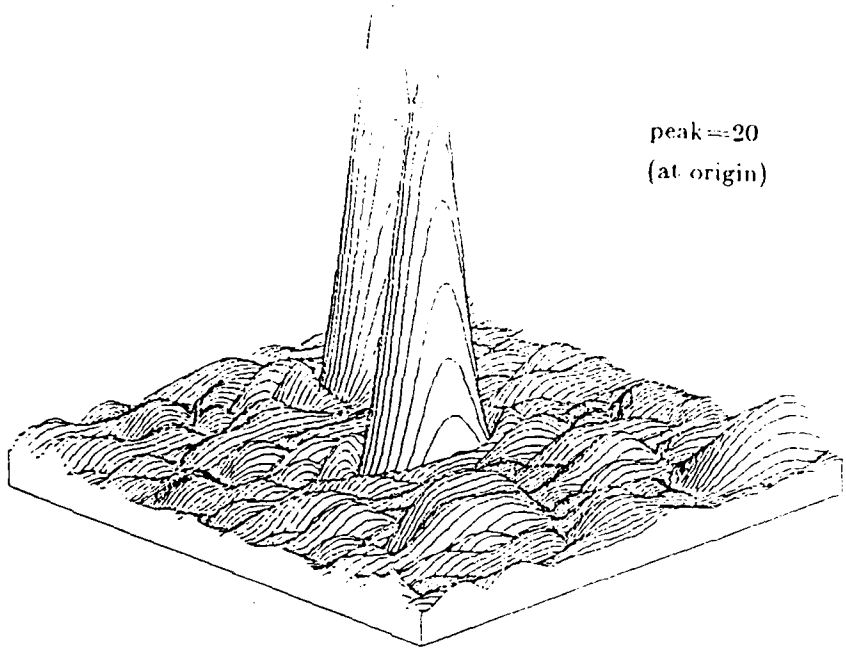

Figure 3-12: Correlation of tank with OBPOF(re)
in the non-centered case.

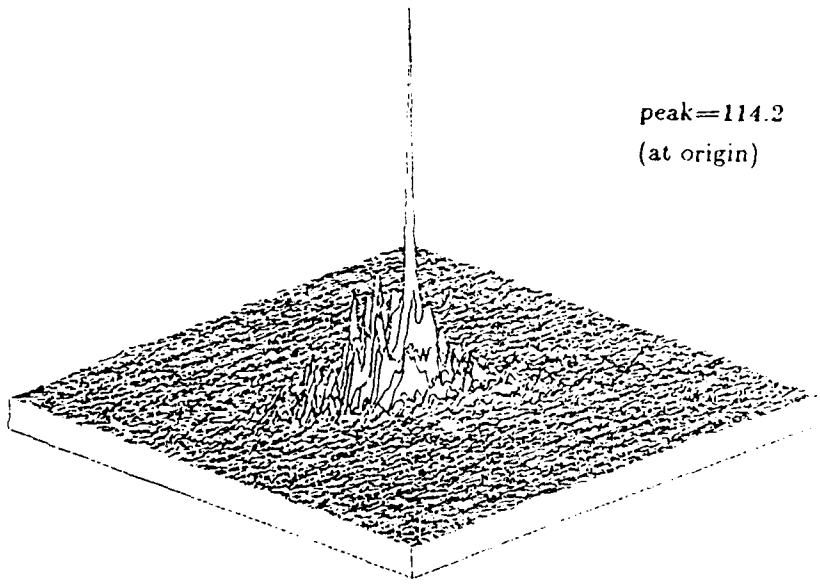

Figure 3-13: Correlation of tank with BPOF(re)
in the centered case.

3-14 show the correlations with the BPOF and OBPOF, respectively. It can be seen that in this case the second peak has disappeared from both outputs.

A possible explanation of the bifurcation phenomenon is that due to the fact we are

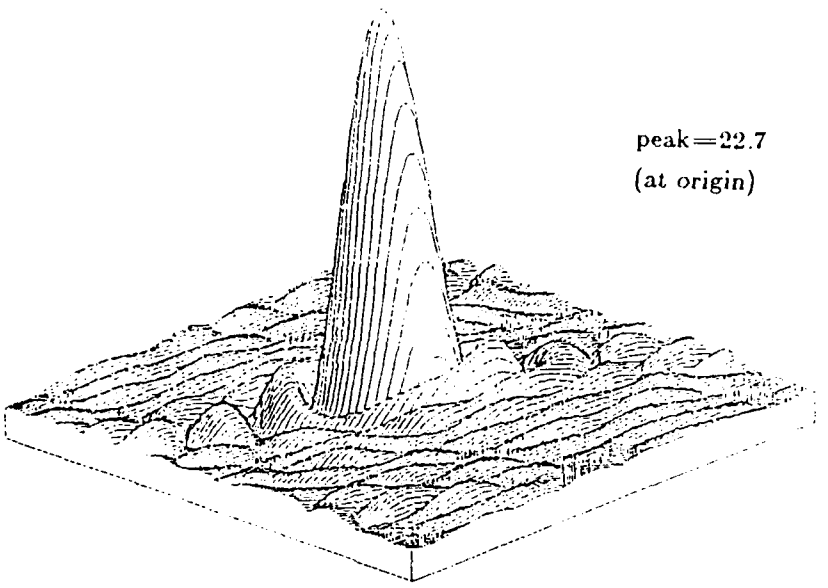

Figure 3-14: Correlation of tank with OBPOF(re) in the centered case.

using the real part of $S(f)$, we are in effect correlating the tank image with its even (if we accept the fact that the binarization operation preserves some of the original information[47]) part. This amounts to correlating the image with itself (i.e., autocorrelation) and with its flipped version (i.e., autoconvolution). When the image is placed at the upper corner of the FFT array, its flipped version is positioned at the other corner across from the center. The fact that there is no overlap between both causes the two peaks to be distinct from one another. On the other hand, in the centered case, both the tank and its flipped version are almost totally overlapping. This causes both peaks also to overlap, appearing as a single peak.

The above argument suggests that by using other binarization schemes instead of the real part, one could perhaps get around this bifurcation problem. In fact, we tested the above simulations using the Hartley BPOF instead. We had little success. Actually, it can be easily argued that using a general binarization provides no guarantee for solving this problem. In all cases we are adding the correlation output to the convolution. The only change the TLA introduces is a scaling factor that is affecting both outputs.

3.7. Distortion Sensitivity of BPOFs and OBPOFs

In this section we present the results of our computer simulations to test the distortion sensitivity of BPOF and OBPOF. As in the POF case, we found that the OBPOF has more tolerance to distortions (rotations) than the BPOF. Fig. 3-15 plots the SNR variations as a function of rotations for both filters using the tank image (centered prior to solving for the filters). The binarization with respect to the real part has been used. In Fig. 3-16 we incorporated the results of the MSF, POF, and OPOF obtained from

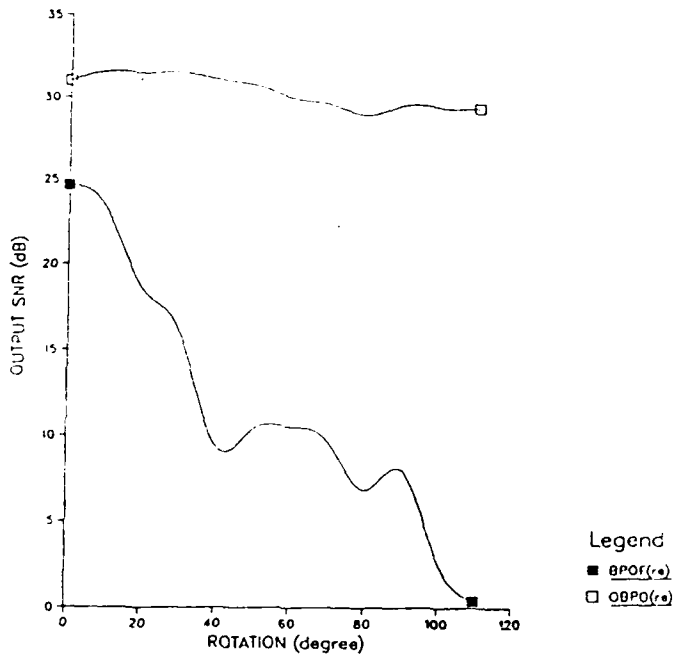

Figure 3-15: Output SNR (vs) rotation for BPOF(re) and OBPOF(re) using centered tank image.

the previous chapter as a reference. It can be observed that the MSF, OPOF, and OBPOF seem to be the least sensitive to input distortions. At the bottom of the scale are the POF and BPOF which exhibit a much more sensitive behaviour. Actually, the POF, even though quite sensitive, seems to keep an SNR margin over the BPOF. This appears to be a direct result of binarization. Finally, the hierarchy introduced earlier (i.e., MSF followed by OPOF, OBPOF, POF, and lastly BPOF) can be seen with no input rotation. Similar

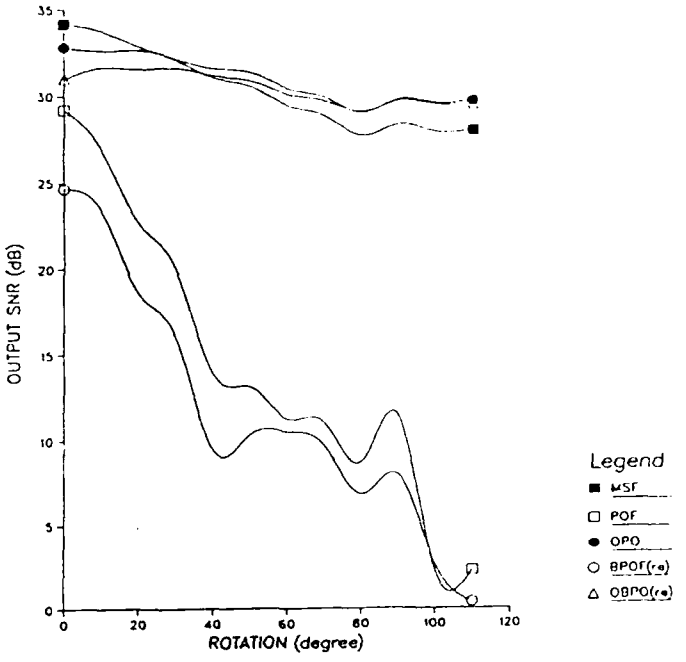

Figure 3-16: Output SNR (vs) rotation for MSF, POF, OPOF, BPOF(re), and OBPOF(re) using centered tank image.

results were also obtained for the pliers image. They further support the sensitivity of BPOF with respect to OBPOF. The details will be omitted for the sake of conciseness.

3.8. Summary

In this chapter we have essentially extended our previous results to binary phase-only filters. We presented two efficient algorithms for the design of BPOFs. These are generalizations of the earlier algorithms. We also presented simulation results that closely agree with the numerically computed results. We have shown, using tank and pliers image examples, that careful selection of the support can improve the SNR by about 5 dB compared to the unoptimized BPOFs. In contrast, selecting the proper TLA seems to affect the light efficiency noticeably while providing an SNR increase of only 1 dB.

We established a link between the design of optimal BPOFs and POFs. This turned out to be quite useful. First, it provided us with another very efficient algorithm. This lead

to a reduction in CPU time by a factor of about 8. This is because the POF algorithm, unlike the BPOF, does not perform its optimization on a grid. However, this algorithm is capable of generating only information pertinent to the optimal BPOF. It does not allow the variations of SNR and light efficiency with respect to the TLA to be monitored. This could be important in situations where trade offs between SNR and light efficiency need to be made. In this case, the other two algorithms should be used. Furthermore, this bridge between BPOF and POF design also allowed us to take advantage of available results related to support selection. Hence, the effect of the detector noise on the BPOF support design is the same as that for the POF. Likewise, the window approximation of the support of POF can be extended to the BPOF case. Typically about 1.5 dB loss in SNR is expected by this approximation.

The bifurcation issue was also addressed. This phenomenon strongly depends on the position of the input image in the FFT array at the time the filters are synthesized. This was illustrated by showing some computer generated output correlations. The TLA does not seem to have a noticeable effect on the bifurcation phenomenon. Finally, we provided some simple computer simulations that test the distortion sensitivity of BPOFs and OBPOFs. As in the POF case, the BPOF was found to be much more sensitive to input rotation than the OBPOF. This appears to be a direct consequence of the implicit high frequency amplification in BPOFs.

In conclusion, it seems that when sufficient light is available, the support function of any BPOF should be optimized using the algorithms we provided. Moreover, our results also indicate that the choice of $\theta = 0^\circ$ for TLA may be a very good choice for most images since most realistic images have more energy in their even parts compared to the odd parts.

Chapter 4

Conclusion

Our research results presented here have significant implications regarding the use of POFs and BPOFs. Most previous research has been somewhat empirical and our efforts have produced some general observations.

Where POFs are to be employed, we strongly recommend using an appropriate masking or support function. While the exact improvements are image-dependent, we seem to obtain about 5 dB SNR improvement by using OBPOFs. Since POFs are expected to function in noisy environments, we must use OPOFs to combat the noise effect. A side benefit of using OPOFs is the reduced sensitivity to input distortions. A disadvantage of using OPOFs is the reduced light efficiency because of the size of the support function. The OPOFs can be implemented in practice in many different ways. One such method is to use a sandwich of a phase-only device and an on-off device in the frequency plane.

More important (from the practical viewpoint) are the OBPOFs. Strictly speaking, OBPOFs are three-valued (+1, 0, and -1). These can be implemented using SLMs capable of 3 levels. Recently, Kast et. al.[32] demonstrated that MOSLMs can be used as a 3-level device. We have shown that substantial improvements in output SNR can be obtained by using OBPOF instead of the conventional BPOF. As in the case of OPOFs, light efficiency is reduced and distortion sensitivity is improved.

The results of this research effort are very encouraging as far as the roles of OPOFs and OBPOFs in practical systems are concerned. We believe that use of optimal filters in improved SLMs will bring the optical correlator into a practical reality.

References

1. A. Vander Lugt, "Signal detection by complex spatial filtering", *IEEE Transactions on Information Theory*, Vol. 10, 1964, pp. 139-145.

2. J. L. Horner and P. D. Gianino, "Phase only matched filtering", *Applied Optics*, Vol. 23, March 1984, pp. 812-816.

3. D. Psaltis, E. G. Paek, and S. S. Venkatesh, "Optical image correlation with a binary spatial light modulator", *Optical Engineering*, Vol. 23, 1984, pp. 698-704.

4. J. L. Horner and J. R. Leger, "Pattern recognition with binary phase-only filters", *Applied Optics*, Vol. 24, 1985, pp. 609-611.

5. M. W. Farn and J. W. Goodman, "Optimal binary phase-only matched filters", *Applied Optics*, Vol. 27, 1988, pp. 4431-4437.

6. W. E. Ross, D. Psaltis, and R. H. Anderson, "Two-dimensional magneto-optic spatial light modulator", *Optical Engineering*, Vol. 22, July/August 1983, pp. 485-490.

7. D. G. Gibson, "Progress in spatial light modulator performance: a status report", *Optics and Laser Technology*, Vol. 20, February 1988, pp. 25-28.

8. D. A. Gregory, R. D. Juday, J. B. Sampsell, R. O. Gale, R. W. Cohn, and S. E. Monroe, Jr., "Optical characteristics of a deformable mirror spatial light modulator", *Opt. Lett.*, Vol. 13, 1988, pp. 10.

9. P. D. Gianino and J. L. Horner, "Additional properties of the phase-only correlation filter", *Optical Engineering*, Vol. 23, 1984, pp. 695-697.

10. J. L. Horner and H. O. Bartelt, "Two-bit correlation", *Applied Optics*, Vol. 24, 1985, pp. 2889-2893.

11. D. M. Cottrell, R. A. Lilly, J. A. Davis, and T. Day, "Optical correlator performance of binary phase-only filters using Fourier and Hartley transforms", *Applied Optics*, Vol. 26, 1987, pp. 3755-3761.

12. J. L. Horner and P. D. Gianino, "Applying the phase-only filter concept to synthetic discriminant function correlator filter", *Applied Optics*, Vol. 24, 1985, pp. 851-855.

13. X. Su, G. Zhang, and L. Guo, "Phase-only composite filter", *Optical Engineering*, Vol. 26, 1987, pp. 520-523.

14. J. Rosen and J. Shamir, "Distortion-invariant pattern recognition with phase filters", *Applied Optics*, Vol. 26, 1987, pp. 2315-2319.

15. R. R. Kallman, "Direct construction of phase-only filters", *Applied Optics*, Vol. 26, 1987, pp. 5200-5201.

16. H.L. Van Trees, *Detection, Estimation, and Modulation Theory, part I*, Wiley, 1968.

17. A. V. Oppenheim and R. W. Schafer, *Digital Signal Processing*, Prentice-Hall, 1975.

18. C. S. Anderson and R. C. Anderson, "Comparison of phase-only and classical matched filter scale sensitivity", *Optical Engineering*, Vol. 26, 1987, pp. 276-279.

19. F. M. Dickey and K. T. Stalker, "Binary phase-only filters: Implications of bandwidth and uniqueness on performance", *OSA Annual Meeting*, Rochester, New York, October 1987.

20. G. A. Korn and T. M. Korn, *Mathematical Handbook for Scientists and Engineers*, McGraw-Hill, 1968.

21. J.A. Bate, M.S. Doyle, and H.J. Ferch, *Computer Programming and Data Structure Using Pascal*, Charles Babbage Research Centre, 1982.

22. R. Conway and D. Gries, *An Introduction to Programming: A Structured Approach Using PL/I and PL/C*, Winthrop Publishers, inc., Cambridge, MA, 1979.

23. D. Casasent and A. Furman, "Sources of correlation degradation", *Applied Optics*, Vol. 16, June 1977, pp. 1652-1661.

24. J. L. Horner, "Light utilization in optical correlators", *Applied Optics*, Vol. 21, 1982, pp. 4511-4514.

25. D. Casasent, "Spatial Light Modulators", *Proc. IEEE*, Vol. 65, 1977, pp. 143-157.

26. D. L. Flannery, J. S. Loomis, and M. E. Milkovich, "Design elements of binary phase-only correlation filters", *Applied Optics*, Vol. 27, 1988, pp. 4231-4235.

27. R. R. Kallman, "Optimal low noise phase-only and binary phase-only optical correlation filters for threshold detectors", *Applied Optics*, Vol. 25, December 1986, pp. 4216-4217.

28. F. M. Dickey, J. J. Mason, and K. T. Stalker, "Analysis of binarized Hartley phase-only filter performance with respect to stochastic noise", *Proceedings of SPIE*, Vol. 938, 1988, pp. 266-279.

29. D. L. Flannery, J. S. Loomis, and M. E. Milkovich, "Transform-ratio ternary phase-amplitude filter formulation for improved correlation performance", *Applied Optics*, Vol. 27, 1988, pp. 4079-4083.

30. F. M. Dickey, K. T. Stalker, and J. J. Mason, "Bandwidth considerations for binary phase-only filters", *Applied Optics*, Vol. 27, 1988, pp. 3811-3818.

31. B. V. K. Vijaya Kumar, "Signal-to-Noise Ratio (SNR) loss in correlators using real filters", *App. Opt.*, Vol. 28, 1 September 1989.

32. B. A. Kast, M. K. Giles, S. D. Lindell, and D. L. Flannery, "Implemetation of ternary phase amplitude filters using a magnetooptic spatial light modulator", *Applied Optics*, Vol. 28, 1989, pp. 1044-1046.

MISSION
of
Rome Air Development Center

RADC plans and executes research, development, test and selected acquisition programs in support of Command, Control, Communications and Intelligence (C^3I) activities. Technical and engineering support within areas of competence is provided to ESD Program Offices (POs) and other ESD elements to perform effective acquisition of C^3I systems. The areas of technical competence include communications, command and control, battle management information processing, surveillance sensors, intelligence data collection and handling, solid state sciences, electromagnetics, and propagation, and electronic reliability/maintainability and compatibility.